



This is a repository copy of *A study of the impact of building geometry on the thermal performance of road pavement solar collectors*.

White Rose Research Online URL for this paper:  
<http://eprints.whiterose.ac.uk/104585/>

Version: Accepted Version

---

**Article:**

Binti Mohd Nasir, S.D.N., Hughes, B.R. and Calautit, J.K. (2015) A study of the impact of building geometry on the thermal performance of road pavement solar collectors. *Energy*, 93 (2). pp. 2614-2630. ISSN 0360-5442

<https://doi.org/10.1016/j.energy.2015.09.128>

---

Article available under the terms of the CC-BY-NC-ND licence  
(<https://creativecommons.org/licenses/by-nc-nd/4.0/>)

**Reuse**

This article is distributed under the terms of the Creative Commons Attribution-NonCommercial-NoDerivs (CC BY-NC-ND) licence. This licence only allows you to download this work and share it with others as long as you credit the authors, but you can't change the article in any way or use it commercially. More information and the full terms of the licence here: <https://creativecommons.org/licenses/>

**Takedown**

If you consider content in White Rose Research Online to be in breach of UK law, please notify us by emailing [eprints@whiterose.ac.uk](mailto:eprints@whiterose.ac.uk) including the URL of the record and the reason for the withdrawal request.



[eprints@whiterose.ac.uk](mailto:eprints@whiterose.ac.uk)  
<https://eprints.whiterose.ac.uk/>

1 **A Study of the Impact of Building Geometry on the Thermal Performance**  
2 **of Road Pavement Solar Collectors**

3 **Diana SNM Nasir <sup>a\*</sup>, Ben Richard Hughes <sup>a</sup>, John Kaiser Calautit <sup>a</sup>**

4  
5 <sup>a</sup> Energy 2050, Department of Mechanical Engineering, The University of Sheffield, Sheffield, S1 3JD, United Kingdom

6 \* Corresponding author. Email: [sdnbintimohdnasir1@sheffield.ac.uk](mailto:sdnbintimohdnasir1@sheffield.ac.uk); Tel. +44(7) 424 289 937

7  
8 **Abstract**

9 Studies on Road Pavement Solar Collectors (RPSC) have shown the potential of reducing the urban  
10 heat island (UHI) effects by dissipating the heat from the pavement for energy harness. Several works  
11 have shown that the generated heat could be utilised for sustainable urban energy system. However,  
12 none of the previous literatures have assessed the effect of building geometry on the performance of  
13 the RPSC. This study investigates the thermal performance of an urban-integrated RPSC system by  
14 using CFD simulation of integrated RPSC system with a standard urban canyon domain and an empty  
15 domain.-Based on 21<sup>st</sup> June at 13:00, it was found that the RPSC system in urban canyon domain was  
16 on average 36.08% more effective in thermal collection and provided on average 27.11% more  
17 surface temperature reduction as compared to the RSPC application in rural/flat domain. The RPSC  
18 performance based on the effect from daily solar intensity was initiated with results demonstrated the  
19 efficiency of the RPSC in an urban setting was 7.14% to 63.26% more than the rural/flat setting.  
20 Simulations of various wind speeds in summer day(s) and the impact of seasonal changes to the RPSC  
21 system were also conducted to investigate the deficiency factors to the system.

22  
23 **Keywords:** CFD, road solar collector, hydroponic pipes, urban canyon, thermal collection, UHI

24  
25 **Number of words: 7130**

# 1 Nomenclature

2

<b>Term</b>	<b>Description</b>
$T_a$	Reference air temperature at z-direction, 293 K
$T_{s,x}$	Reference ground surface temperature at z-direction, 352 K
$T_{w(i)}$	Average water inlet temperature, K
$T_{w(o)}$	Average water outlet temperature, K
$U_H$	Velocity at different height at z-direction, m/s
$c_a$	Concentrated canyon area
$k_s$	Sand-grain roughness height, m
ABL	Atmospheric boundary layer
ASC	Asphalt solar collector
Delta T	Difference in average water outlet temperature and average water inlet temperature, K
DO	Discrete Ordinate
H	Building height, m
PTC	Potential thermal collection, %
RPSC	Road pavement solar collector
RPSC-0	Road pavement solar collector simulated in rural/flat domain
RPSC-1	Road pavement solar collector simulated in urban domain
STR	Surface temperature reduction, %
T	temperature K
UHI	Urban Heat Island
UTC	Universal Time Coordinated
W	Building width, m
$C_s$	Roughness constant
$k - \varepsilon$	K-epsilon
$U_0$	Velocity at reference, m/s
$z_0$	Aerodynamic roughness

3

4

5

6

7

8

9

## 1    **1        Introduction and previous related works**

2    Urban Heat Island (UHI) effect is a form of accumulated heat caused by urbanisation when buildings,  
3    roads and other infrastructure elements replace open land or water areas. These elements tend to  
4    absorb the heat from the sun rather than reflect it, causing the surface temperature and air temperature  
5    to elevate [1]. It is a phenomenon where significant temperature difference between inner areas of a  
6    city and their neighbouring areas can be perceived. The rise in temperature is between 3°C to 6°C  
7    during calm and clear sky with different intensities obtained when a climate factor is considered [2,  
8    3]. Several studies [4, 5] predicted that the rise in air temperature will be doubled within 50 years. A  
9    field study [6] showed evidence of an increase in the UHI intensity by 1.5°C after a two decade  
10    measurement. The result demonstrated how the urbanisation of a city evolved by time and contributed  
11    to warm the city. This significant increase in the urban temperatures affects the consumption of  
12    cooling energy to achieve thermal comfort in buildings [7]. This also leads to the increase in global  
13    emission and generation of urban pollutants [8, 9].

14  
15    A study [10] conducted during the summer period revealed that the exposed urban surfaces i.e. ground  
16    pavements and building roofs can be 27°C to 50°C warmer than the ambient air temperature.  
17    Solutions such as the replacement of artificial surfaces with natural surfaces were initially proposed to  
18    improve the albedo of the urban surfaces [7]. Apart from the significant impact of higher surface  
19    albedo on the surrounding environment, consideration of not compromising the outdoor pedestrian  
20    thermal comfort was highlighted using an Index of Thermal Stress [11]. Field monitoring data and  
21    meteorological simulations carried out by [12] suggested that the increase in the surface albedo is an  
22    effective way of diverting the heat island intensity in the urban area. However, the impact of  
23    anthropogenic heat was found relatively nominal for residential and commercial areas. A ‘cool  
24    communities’ under the US Department of Energy in Loss Angeles demonstrated that by reroofing  
25    and repaving in lighter colours could result in huge savings in cooling expenses [13].

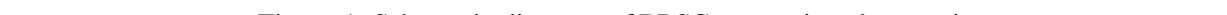
26  
27    An experimental study [14] in the early 90s measured and compared the heat output from several  
28    types of surface materials and established options of alternative material to improve the surroundings  
29    thermal environment. A laboratory test was conducted to investigate the passive energy storage of a  
30    horizontal concrete slab based on the heat transfer from two major parameters, the solar heat flux and  
31    the ambient temperature. The study demonstrated huge impact of natural convection on the surface  
32    radiation heat loss which is up to 40% [15]. Later on, concern on the lack of data on the asphalt  
33    thermal properties was raised [17] and the underestimation of the heat convection coefficient can  
34    cause an over prediction of the pavement temperature [18]. Simulation on predicting the impact of  
35    thermal properties of pavement slabs was carried out [19, 20] and studies found that the asphalt  
36    pavement type can be heated as high as 70°C during hot summer days [21]. The heating of the road  
37    and pavement surfaces were related to the formation of UHI effect [22, 23] and techniques of

1 reducing the effect were thoroughly discussed. Several works [23, 24, 25] have proposed the use of  
2 Asphalt Solar Collector (ASC) system to solve the limitation of asphalt pavements. The ASC is the  
3 application of heat exchanger between the surfaces and the downward pavement layers for the  
4 purpose to absorb the temperature and convert it into the form of thermal energy [23]. A hydronic  
5 ASC system was initially proposed for ice/snow melting technique during winter season [27].  
6 Prediction of the system efficiency was carried out by using computational modelling [23], laboratory  
7 imitated simulation [28] and laboratory testing [29]. Limitations of the system were highlighted on the  
8 pavement structural stress formation around the circulated pipes [26] and the potential pipe leaking  
9 [31, 32]. Thus, alternative options were studied and the prototypes were tested to overcome the  
10 limitation [31, 32].

11

12 This study presents an investigation of a hydronic pipe collector integrated into a roadway in an urban  
13 scenario. Despite the limitation of using hydronic pipes in urban areas, a water element is a common  
14 medium applied for urban water heating supply. For future sustainable use, this study emphasised a  
15 system that has dual functions: (i) To reduce ground surface temperature and (ii) to be used as an  
16 energy collection system i.e. water heating supply. Figure 1 shows the schematic diagram of an urban  
17 street canyon with the RSPC system.

18

19  Figure 1: Schematic diagram of RSPC system in urban environment

20

21 The primary reason of highlighting the potential development of integrated urban road solar collector  
22 is due to the evidenced high temperatures in urban areas. The urban geometry influences the solar heat  
23 flux more than the flat terrain due to its complex shapes; which causes heat to accumulate during the  
24 multiple reflections of the photons to the sky [7, 33]. Investigation of air temperature based UHI  
25 effect was demonstrated by using the aspect ratio of a street canyon height to the width,  $H/W^1$ ; with  
26 higher aspect ratio was evidenced to decelerate the reflection of long-wave emission from the ground  
27 surface [33, 43]. A simplified 2-D mathematical model was developed to evaluate the impact of street  
28 canyon aspect ratio in increasing the air based UHI effect by comparing to the one without canyon  
29 [34]. Recent studies highlighted the extensive use of numerical modelling for urban microclimatic  
30 related issues. Computational Fluid Dynamic (CFD) software has the flexibility to model an urban  
31 geometry scale in higher resolution [40]. To replicate an urban canyon, a simplified urban canyon  
32 with longer configuration was chosen [39] but multiplication of canyon geometry was preferable for  
33 the comparison [36]. It was found the computational codes have the ability to carry out prediction  
34 analysis on air flow modification in the combined tall buildings with narrow street canyon for UHI  
35 mitigation [38]. In the study of [35], the initiative to apply ‘cool’ surface coating to mitigate the UHI

---

<sup>1</sup> Street canyon aspect ratio,  $H/W$  is a ratio of building height,  $H$  (m) to the width of a street canyon,  $W$  (m) [34]

1 effect in deep canyon was highlighted. CFD simulations of deep street canyon were initially validated  
2 by the collected mobile meteorological data. A similar approach was found in [39] that presented a  
3 CFD street canyon simulation which was validated with the wind tunnel laboratory tests of [42]. This  
4 study [39] highlighted the effect of 3-D solar radiation using Solar Ray Tracing to the air flow and  
5 thermal within the canyon. Coupling CFD and BES models were conducted in [36], highlighting BES  
6 was used to provide initial boundary conditions i.e. the temperatures of building and ground surfaces  
7 meanwhile CFD was used in predicting the temperature and the air flows. The CFD-based ENVI-met  
8 model was compared by [30] with the ADMS-Temperature and Humidity model to evaluate the  
9 prediction of urban air temperature. Underestimation of sensible heat flux was found in ADMS-TH  
10 meanwhile CFD-based ENVI-met underestimated the turbulent momentum and thermal diffusivity.  
11 Nevertheless, the temperature measurements i.e. façade temperatures at the concentrated field areas  
12 were well predicted in CFD simulation although it underestimated/overestimated results due to  
13 geometry simplification [37].

14

15 For this study, we highlighted the gap based on the previous literatures which have not included  
16 building geometry in evaluating the performance of road pavement solar collector (RPSC). Three  
17 probabilities can affect the estimated water temperature collection in an urban scenario: (i) Buildings  
18 will cause un-even temperature distribution inside the canyon and affect the thermal performance of  
19 RSPC; i.e. RSPC pipes below surfaces covered by building shadows will receive less heat [45], (ii)  
20 solar reflection between buildings can further increase the temperature of the ground surface, and (iii)  
21 the performance of the RSPC will vary depending on the time of the day. 3-D numerical simulation of  
22 a hydronic pipe collector system for embedded in a ground surface between two buildings was carried  
23 out. A simplified form of urban model developed by Bottillo et al. (2014) [39] was used as a  
24 benchmark geometry. Two RPSC scenarios were compared; with buildings for urban and without  
25 buildings for rural/flat. The RPSC can function as the future sustainable practical mitigation technique  
26 of air-surface temperature based UHI effect despite its main function as an energy collection system.  
27 The model developed here can be used to assess the impact of the location of RPSC, solar pattern,  
28 airflow, material properties and shape of buildings on its performance.

29

## 30 **2 De-coupled computational modelling approach**

31 This study presents a de-coupled computational modelling method to analyse the effect of building  
32 geometry on thermal performance of RPSC system. A benchmark model [39] which represents a  
33 simplified urban street canyon model in a computational flow domain was selected. Two separate  
34 domains were classified as macro domain and micro domain. The macro domain represents a ground  
35 road surface between two buildings. This model was constructed with two sub-objectives: (i) to  
36 obtain validation of atmospheric boundary layer (ABL) profile, canyon air velocity profile and canyon  
37 air temperature profile from a benchmark model of [39]; and (ii) to obtain the simulation output of

1 road surface temperature profile. Prolong to achieve the second sub-objective; the simulation output  
2 of (ii) was used as the boundary conditions for the micro domain simulation which consisted of an  
3 embedded RPSC system. Combined macro-micro model in one domain requires high computational  
4 time in order to obtain optimal results with optimal mesh sizing. Thus, de-coupled modelling  
5 approach was selected for this study to achieve cost and time effectiveness. A flow chart of the  
6 integrated numerical methodology is shown in Figure 2.

7  
8 Figure 2: Methodology chart of the de-coupled approach CFD model

## 9 10 **2.1 Computational domain**

11 This section details the computational modelling of the macro domains and the micro domain.

### 12 13 2.1.1 Urban macro domain (RPSC-1)

14 A street canyon model consists of a 20m width road in between two rows of buildings; each with the  
15 dimension of 100m length, (L) 20m width (W) and 20m height (H). Canyon aspect ratio (H/W) was  
16 described as 1. Cross-sectional image of characterised street canyon was visualised in Figure 3.

17  
18 Figure 3: Schematic diagram of RPSC-canyon system

19  
20 Building geometry influences the wind air flow and its speed from inlet(s) direction meanwhile  
21 building walls which face one another act as the vertical surfaces to influence solar reflectivity and its  
22 energy scheme in a canyon. Figure 4 represents the characterisation of macro domain with optimal  
23 dimension guidelines as set by [39].

24  
25 Figure 4: Urban domain description based on height from plan view

26  
27 Simulating a computational urban model has several challenges. For an air flow simulation as referred  
28 to Bottillo et al. (2014), it is essential for the outflow distance to be three times larger than the inflow  
29 distance in order to reduce computational uncertainties due to reversed outflow. This is also applied  
30 for the distance between the building roof top and the top plane of the domain which requires  
31 sufficient height so the air flow will over through without causing flow errors at the respective canyon  
32 area. In the macro model, three volumes were divided: (i) air-fluid region (wind flow), (ii) 5m depth  
33 solid region (road and soil) and (iii) empty region (building interiors; excluded in the study). In this  
34 study, the wind inlet plane was oriented parallel to  $y$ -direction, creating the first building wall closer  
35 to the inlet plane acts as an obstacle to the constant wind thus encourage the turbulent development.  
36 This study only considered one long street canyon shape with one building orientation.

### 2.1.2 Flat/rural macro domain (RPSC-0)

Similar guidelines applied for the urban macro domain were also applied for the empty macro domain which represents a less dense urban area or a rural area. In this domain, only two regions were divided: (i) air-fluid region (wind flow), and (ii) 5m depth solid region (road and soil). Similar location and distances of direction  $x$ ,  $y$  and  $z$  were indicated for the canyon ground road surface. The only difference is the ground road surface was not sandwiched between two buildings, which indicated there is no influence of building geometry to the temperature of the road surface. In previous studies, comparative analysis was demonstrated to evaluate the UHI intensity between these two scenarios [34]. This study carried out similar comparisons to evaluate thermal performance of the RPSC system by providing selected boundary conditions as detailed in Section 2.3. As total, the size of both macro domains was set as 460m length  $\times$  300m width  $\times$  125m height including 5m depth below ground surface.

### 2.1.3 RPSC embedment and micro domain

RPSC system was setup by locating 19 circular hollow horizontal 10m length copper pipes with 0.005m wall thickness and 20mm diameter [28] beneath the ground road surface at the depth of 0.15m. The distance between the pipes was indicated as 1m. The system was designed by layering the pipe length parallel to the road. In order to simplify the model and reduce the computational time; the RPSC pipes were only added to the central area, approximately 10% of the total ground road surface (see Figure 12). The total area for the 19 embedment pipes was approximately 10m length  $\times$  20m width. A micro domain was designed with the pipes embedded inside a solid ground of 10m length  $\times$  1m width  $\times$  0.3m ground depth, representing the simulation model of the total 19 pipes. The pipe location was at the centre of the solid ground, which means the side by side distance was 0.5m.

## 2.2 Mesh

Patch independent hybrid meshing technique was applied on all investigated geometries. The patch independent mesh algorithm is based on the subsequent spatial subdivision algorithm which ensures refinement of the mesh where essential, but retains larger elements where feasible, therefore allowing faster computational times.

### 2.2.1 Macro domains

For the macro domain, edge sizing was used to refine the mesh sizing concentrated at the canyon parts,  $c_a$ : (i) canyon ground road surface, (ii) building walls, and (iii) canyon lower ground. Inflation of First Layer Thickness option was applied by indicating 0.1m for the first layer thickness with growth rate of 1.2 and maximum layer of 20 numbers. Figure 5(a) shows the generated mesh based on this setting. The inflated layers sized differently by the increased thickness from one layer to another; creating hexahedral meshes close to the canyon ground as Figure 5(b).

1 Figure 5: Perspective view of (a) canyon mesh generation (b) hexahedral mesh at building wall

2

3 Similar boundary conditions were also applied for the macro domain of flat surface (no building).  
4 Cross-sectional plane at the centre of the length of ground road surface was created to compare  
5 between urban macro domain and flat/rural macro domain. The controlled inflation setting and edge  
6 sizing generated similar growth rate of the mesh sizing for both models.

7

### 8 2.2.2 Micro domain

9 For the micro domain, the pipe body meshing was sized 0.020m; dividing the total length into 2000  
10 elements with 0.005m sizing each. This setting generated 0.020m × 0.02m hexahedral typed of mesh  
11 for upper and lower layers with thickness reduction for the layers closer to the pipe body.

12

### 13 2.2.3 Mesh independence test

14 In order to verify the accuracy of the numerical models, a mesh independency test was carried out to  
15 determine the variation in results over increasing mesh sizes. Basic concepts associated with mesh  
16 refinement deals with the refinement and evaluation of elements where the posterior error indicator is  
17 larger than the preset criterion, while mesh enrichment considers running higher order polynomials till  
18 the solution is expected to improve with a fixed mesh [41]. Mesh verification was carried out using  
19 mesh refinements (h-method) in order to optimise the distribution of mesh size, h over a finite element  
20 [41]. Different edge sizing values were applied at  $c_a$  to indicate the mesh was sized in coarse, medium  
21 and fine [51]. Three edge sizing of 1.00m, 0.50m and 0.25m were determined and described in details  
22 as Table 1.

23

24 Table 1: Mesh setting based on edge sizing

25

26 Average temperature of three points were measured based on the distance of 2m away from the  
27 canyon centre coordinate at every axis (x-axis 150m, y-axis 130m and z-axis 0m) of the urban macro  
28 domain and the result was shown in Figure 6.

29

### 30 Figure 6: Mesh independent test

31

32 This test was carried out to observe the temperature dependency based on the mesh sizing. The  
33 temperature point taken at 2m distance away from the canyon centre x-coordinate indicated the  
34 increased rate was 0.106% between coarse mesh and medium mesh and 0.321% between medium  
35 mesh and fine mesh. For the temperature point at 2m distance away the canyon centre y-coordinate,  
36 higher difference can be observed but not less than 0.325% (between medium mesh and fine mesh)  
37 and not more than 0.548% (between coarse mesh and medium mesh). The z-coordinate temperature

1 points of the three mesh sizing were plotted pretty linear with less than 0.032% difference from coarse  
2 to fine. Overall, the average temperature dependency on mesh sizing was nominal thus the validation  
3 for hybrid meshing can be carried out to compare with the previous benchmark model [39]. Fine mesh  
4 model was selected with total elements of 2,063,739 and total nodes of 659,968. High speed  
5 computational time could still be achieved, although this hybrid mesh sizing generated the highest  
6 total elements and nodes. For rural/flat domain, fine mesh model with total elements of 2,010,784  
7 and total nodes of 731,198 was used for analysing the comparative studies.

## 9 **2.3 Boundary conditions**

### 11 2.3.1 Study background

12 The model was simulated based on the setting of Milan, an urban centre of Italy [39]. This city is  
13 located in north Italy with longitude 9.18°E, latitude 45.47°N and UTC +1. The summer season in  
14 Milan is a mix of hot temperature and low winds [50]. Similar boundary as [39] was applied. The  
15 solar load module was set to a summer day in June [39]. To simulate the ambient temperature during  
16 the 21<sup>st</sup> of the month, the inlet air temperature was set to 303K (30°C) [39]. According to [39], a  
17 constant velocity of 2 m/s at turbulence intensity of 10% was initially set while the value of  
18 aerodynamic roughness  $z_0$  for the ground surface was calculated based on the sand-grain roughness  
19 height  $k_s$  of 1.0 m and roughness constant  $C_s$  of 0.5m as suggested by Blocken et al. (2007) [43] as  
20 shown in Equation 1:

$$22 \quad z_0 = \frac{k_s \cdot C_s}{9.793} \quad (1)$$

24 The simulation assumed the first row of building located close to the wind inlet plane as Building A  
25 and another building row located parallel to Building A is Building B. Similar boundary conditions  
26 were applied for both building walls. Material characteristics of the canyon road surface, building  
27 walls and RPSC system are described in Table 2. The simulation was carried out at 13:00 hour for  
28 both macro domains to demonstrate the potential high sun exposure on the road horizontal surface. 19  
29 pipes were depicted to be layered underneath canyon road surface at the centre canyon region with 1m  
30 gap between two pipes. For the comparative analysis of two separate macro domains, only 9 pipes  
31 were selected every two pipes gap (2m distance centre-to-centre). The random selection was made  
32 from the very centre pipe location (pipe C-1) towards building wall A (A-2, A-3, A-4, A-5) and  
33 towards building wall B (B-2, B-3, B-4, B-5) as shown in Figure 7. The pipe water velocity of 0.1 m/s  
34 [44] was set at the inlet plane with temperature 293K (20°C).

36 Table 2: Boundary condition applied to wall surfaces [39, 41]

1 Figure 7: RPSC pipes embedded inside (a) a canyon road surface (b) flat surface without canyon

### 2 3 2.3.2 Daily time-dependent simulation

4 This study also analysed the effect of solar intensity in every hour of steady-state simulation limited  
5 between 10:00 in the morning until 15:00 in the afternoon of similar day. This was carried out based  
6 on the assumption that the ground road surface temperature will change according to the changes in  
7 solar radiation. The simulation analysis was based on the 3 pipes selected out of the 9 pipes located  
8 the nearest to the buildings (pipe A-5 and B-5) and the very centre pipe (pipe C-1).

### 9 10 2.3.3 Changes in wind velocity

11 The average maximum wind velocity of the monthly mode in June can reach up to 10.3 m/s with the  
12 average monthly wind speed is less than 2 m/s [46]. Therefore, the velocity influence on the  
13 performance during the 21<sup>st</sup> June at 13:00 hour was investigated by changing the inlet to 1 m/s, 5 m/s  
14 and 10 m/s. The ambient temperature was considered 303K, following [39].

### 15 16 2.3.4 Seasonal comparison

17 In order to investigate the impact of different seasons on the performance of the RPSC, the inlet  
18 conditions were varied based on the average maximum ambient temperature for the 21<sup>st</sup> of March,  
19 June, September and December representing the spring season, summer seasons, autumn season and  
20 winter season, respectively. The temperature values were calculated based on the climate data from  
21 weather station of Cavaria Con Premezzo located at the longitude 8.809°E and the latitude 45.689°N  
22 [47, 48, 49]. The seasonal effect was being investigated with the constant wind velocity of 2 m/s.  
23 Table 3 displays the seasonal ambient temperature values for the prediction of surface temperature,  
24 outlet water temperature and the Delta T for the pipe.

25  
26 Table 3: Seasonal maximum ambient temperature on 3-month basis [46, 47, 48, 49]

## 27 28 **2.4 CFD model**

29 This study emphasised on conductive and convective heat transfer by simulating two domains in  
30 ANSYS Fluent 14.0. Discrete Ordinate (DO) model was used to solve transport equations in  $\vec{s}$   
31 direction for fluid flow and energy equations. Solar Ray Tracing of the Solar Load Model was  
32 coupled in order to include the effect of solar radiation in the 3D simulation. Besides its practicality to  
33 be applied as heat sources in energy equations, Solar Ray Tracing supplies direct outside beam  
34 direction and intensity parameters to DO model. It calculates the sun radiation based on global sun  
35 location in the sky at a specified date, time zone, longitude-latitude position and sunshine factor [41].  
36 The principle of momentum, continuity and heat conservation that used pressure and steady RANS  
37 equations were fully considered in order to simulate urban turbulent wind/air flow. The standard

1 steady-state  $k-\varepsilon$  model was used with assumption the wind flow is fully turbulent based on model  
2 transport equation for turbulence kinetic energy ( $k$ ) and dissipation rate ( $\varepsilon$ ) [41]. Radiation model and  
3  $k-\varepsilon$  model solved radiation and convection heat transfer in both macro domains by simulating solar  
4 radiation and wind velocity into the concentrated ground road surface.

### 6 **3 Method validation**

7 This section presents the validation results of the wind profile, air temperature profile and ground  
8 surface temperatures of an urban macro domain.

#### 10 **3.1 Validation of wind velocity and temperature profiles**

11 For the first validation test, wind velocity test was done to generate profiles at four different locations  
12 (00m, 20m, 40m and 60m) as per shown Figure 8. For the validation of urban canyon, the simulation  
13 data and time was taken on 21<sup>st</sup> June at 13:00. The applied roughness on the ground surface created  
14 air-solid friction; causing full development of turbulent wind at the position 60m from the inlet plane  
15 before reaching the first building wall [39]. Based on Figure 8, it can be observed that the velocity  
16 magnitude profiles based on four different locations approaching the first building wall was  
17 comparable to the previous CFD simulation. The results were compared with the CFD modelling of  
18 [39] and wind tunnel experiment carried out by [42]. This validation was done with a wind tunnel  
19 experiment developed by [42]. The given ground surface temperature and air temperature were  
20 initially set 352K and 293K, respectively [39]. The CFD model followed the experimental scale  
21 model of 1:200 and a constant wind velocity of 1.5 m/s was set at the inlet plane [39]. Comparisons of  
22 the dimensionless vertical velocity and temperature profiles at the centre of urban street canyon  
23 (0.65m distance from the inlet point) are shown in Figure 9 and Figure 10, respectively.

24  
25 Figure 8: Validation of wind velocity at four locations based on y-direction

26  
27 Figure 9: Canyon wind velocity profile

28  
29 Figure 10: Canyon air temperature profile

30  
31 Figure 9 shows the comparable air velocity profile of the current model to the previous CFD and wind  
32 tunnel profiles [39]. Very low air velocity was observed closer the ground surface and gradually  
33 increased with the z-height. Simulated canyon air temperature profile (Figure 10) was more  
34 comparable to the wind tunnel air temperature profile [42] with 4.57% difference on average as  
35 compared to the previous CFD simulation [39] with 10.61% difference on average. Good agreement

1 was found without overestimation/underestimation measurement at the ground temperature profile,  
2 resulting good validation for the concentrated area.

### 3 4 **3.2 Validation of ground road pavement temperature**

5 Essential validation of the horizontal ground surface is required for the RPSC thermal performance.  
6 The only available validation data was the simulation dated 26<sup>th</sup> June at 14:00 hour. This validation  
7 compared the temperature results of the three measurement points based on [39]: (i) ground surface  
8 temperature 1m distance from centre of Building A, (ii) ground surface temperature 1m distance from  
9 the centre of Building B, and (iii) external (outside canyon) ground surface temperature. Figure 11  
10 displays the comparison of the ground surface in three points between the previous CFD result and the  
11 current result.

12  
13 Figure 11: Validation of the ground road surface temperatures

14  
15 The temperature at point A validated the previous model gave minimal value, 1.15%; error meanwhile  
16 for the external point, the percentage error was 2.36%. The largest difference was obtained for the  
17 validation of the temperature at point B with 8.85% difference.

## 18 19 **4 Results**

20 Comparative results between the urban model simulations and the rural/flat model simulations are  
21 presented with the following discussion within six sections.

### 22 23 **4.1 Surface temperature contours**

24 ANSYS Fluent solved the temperature of canyon ground road surface for 13:00 hour. This simulation  
25 demonstrated constant temperature all over the surface of rural/flat macro domain. For urban macro  
26 domain, hotter temperature contours were observed at the centre region of the surface and closer to  
27 Building A with lower temperature contours spread from the centre to the northern and the southern  
28 regions of the canyon road surface. Surface temperature was observed not so much diverse at the  
29 sideway of Building B, showing the ground surface temperature was affected by the shadow from  
30 Building B which covered more less one third of the surface area. Figure 12 demonstrates the  
31 comparative result of the surface temperature ranged between 293K and 360K for urban and rural/flat  
32 macro domains.

33  
34 Figure 12: Simulated ground surface temperature in urban and rural/flat macro domains

1 The air flow from the inlet plane moved across the first building (Building A) and penetrated the  
2 canyon area from the top and sides of the canyon. The three cross-sections plot of the airflow velocity  
3 vectors at 120m (left), 150m (centre) and 180m (right) are shown in Figure 13.

4  
5 Figure 13: Air profile at (a) 120m x-direction, (b) 150m x-direction (c) 180m x-direction  
6

7 As expected, low air speed was obtained deep down the canyon, resulting from the blocking effect of  
8 the Building A that has reduced the convective heat transfer from the higher surface temperature to  
9 the lower air temperature. Comparing the three cross-sections, it was noticed more air circulation  
10 seems to be in the section of 120m and 180m *x*-direction. The location that is closer to the opening of  
11 the canyon has higher possibility to receive high velocity wind carrying lower temperature, causing  
12 reduction in the surface temperature. This explains the trend observed for the ground surface  
13 temperature in Figure 12, which shows lower surface temperatures in the left and right corner of the  
14 canyon and higher temperature in the centre of the canyon.

#### 15 16 **4.2 Average surface temperature at selected points**

17 Figure 14 shows a plot of the area weighted average of the ground road surface temperature, 0.15m  
18 above selected pipe location to compare both configurations.

19  
20 Figure 14: Ground surface temperature 0.15m above selected pipe location at 13:00 hour  
21

22 For the urban macro domain (RPSC-1), the temperature varied where the ground road surface  
23 temperature descending from pipe C-1 towards Building B and vice-versa can be observed towards  
24 Building A. Simulation at 13:00 hour demonstrated the solar radiation at the angle where the Building  
25 B becomes a factor for the refraction of the solar angle, causing the shadow effect to reduce the  
26 surface temperature closer to the Building B. higher surface temperature was observed towards the  
27 Building A, due to the less amount of solar blocking on the surface. Different trend was observed for  
28 the rural/flat domain simulation where similar surface temperature was obtained 0.15 m above every  
29 pipe location. The stitched graphics in Figure 15(a) and 15(b) of 9 pipes with temperature ranging  
30 between 293K and 360K compared the surface temperature reduction of urban model and rural/flat.

31  
32 Figure 15: Surface temperature after RPSC simulation at 0.15m below pipes for: (a) urban macro  
33 domain (b) rural/flat macro domain  
34

Based on Figure 15(a) and 15(b); at 13:00 hour, urban simulation displayed unequal temperature reduction from the flowing water inside RPSC pipes. With the constant 0.1 m/s water velocity [44] for all pipes, lower temperature reduction can be observed for the pipes closer to the Building B and higher temperature reduction towards the Building A. Conversely at similar time for rural/flat simulation, equal temperature reduction can be observed for all 9 pipes. This demonstrated the RPSC pipes perform uniquely with buildings as compared to the simulation without buildings.

#### **4.3 Delta T, PTC and STR values**

Average water outlet temperature was calculated by selecting the average weighted area of the pipe outlet plane and the temperature difference of inlet-outlet selection is represented as Delta T. The results for Delta T, Potential Thermal Collection (PTC) and Surface Temperature Reduction (STR) based on the simulation of summer day 21<sup>st</sup> June at 13:00 hour are summarised in Table 4. For RPSC pipes in the urban domain (RPSC-1), it was observed the effect of building shadow can reduce the thermal performance of the RPSC pipes from 16.82% to 34.27%. The obtained minimum PTC values were not less than 3% and the maximum values were not more than 5%. Based on the calculated results, the urban RPSC was 36.08% more efficient as compared to the rural/flat RPSC. As observed in Figure 14 and 15, the urban surface has absorbed heat in a very diverse range which displayed very strong influence of the building geometry to the surface temperature. The reduction of surface temperature demonstrated equal reduction value for all rural/flat RPSC pipes of 9.11%, whereas a significant reduction was observed for the urban RPSC with some locations absorbing more heat. The calculated STR values of the integrated urban RPSC were not less than 9% and not more than 14%; displaying potential of the system to reduce the urban surface temperature 27.11% more than the system applied in the rural/flat surface.

Table 4: Calculated PTC and STR values based on 21<sup>st</sup> June

#### **4.4 Effect of solar intensity on RPSC performance**

This section shows the results of the 6-hour simulation to investigate the effect of the solar intensity on the water outlet temperature during the summer day. Figure 16 plots the water outlet temperature for pipe C-1, A-5 and B-5 for the very centre pipe, the closest pipe to Building A and the closest pipe to Building B, respectively. Similar pipes were selected for rural/flat model and to be plotted in similar figure.

Figure 16: Solar intensity study on outlet water temperature

This comparative study demonstrated that all selected pipes for both models obtained gradual increase in the water outlet temperature from the early morning and achieved highest outlet water temperature at noon before the temperature began fall towards evening. Rural/flat pipe demonstrated similar trend with the urban pipe at every hour simulation, highlighting the temperature difference between the rural/flat pipe and the urban pipe B-5 was obtained as high as 0.62K at 13:00 hour but not as much as the difference to the centre pipe C-1 and pipe A-5 with significant value obtained as high as 4.19K and 5.39K, respectively. Daily simulation analysis has shown the importance of considering the effect of solar intensity to the system performance in an urban domain. In the previous sections, it was found significant to simulate the integration of urban geometry and the RPSC pipes and to compare this configuration with no-building setting. Time-dependence simulation can provide necessary deliberation for the system application to achieve high efficiency.

#### **4.5 Changes in wind velocity during summertime**

In the literature section, it was established that the uncertainty of the wind velocity can be the major factor in influencing the temperature of the surface. According to the weather data in [46], wind velocity can reach up to 10.3 m/s and less than 2 m/s during very less windy days. This study examined the effect of changing the wind velocity during the day of the maximum ambient temperature. Figure 17 demonstrates the plotted values of the simulated surface temperature and the water outlet temperature based on the very centre pipe in the urban canyon, C-1. The results showed that higher wind speeds can significantly reduce the surface temperature and the obtained outlet water temperature. It was also observed the Delta T value was reduced as high as 8.45K from the simulated value of the very less windy state, 1 m/s.

Figure 17: Delta T of RPSC performance based on wind factor

Figure 18 demonstrates the comparative air flow vector profile plotted in between the buildings at the centre location 150m from  $x$ -direction. The lowest wind speed simulated for this study was 1 m/s, and the highest velocity obtained in the canyon was not more than 0.2 m/s. The highest wind speed could be obtained closer to the road surface was not more than 1 m/s. For the highest wind velocity simulated, 10 m/s; the vortex rotation in the canyon was observed moving in clockwise direction with higher velocity closer the walls. Highest velocity (2.8 m/s) was observed above 10m from the ground beside the wall of Building A. As the wind rotated deep down the canyon, the velocity closer the centre road surface was reduced to 2.2 m/s. Based on the simulation; the wind circulation was more significant with high velocity as compared to the low wind velocity, resulting more cooling effect in the canyon space during the windy day. However, it should be noted that higher wind can also limit the RPSC system performance and wind conditions in the area must be considered when designing and integrating into the urban spaces. For example; by locating the RPSC in areas with low wind

speeds, the system can perform effectively in terms of surface temperature reduction and temperature collection.

Figure 18: Cross-sectional plane of velocity vector inside the canyon:

(a) 1 m/s (b) 2 m/s (c) 5 m/s (d) 10 m/s

#### 4.6 Seasonal effect on Delta T

The effect on different seasonal conditions on the RPSC performance is shown in Figure 19. The figure summaries the prediction of the surface temperature above 0.15m from pipe C-1 every 21<sup>st</sup> day during the months of: (i) Spring – March, (ii) Summer – June, (iii) Autumn – September (iv) Winter – December [47, 48, 49]. Based on the simulations, it was predicted that the summertime provided highest surface temperature. The change of the month from 21<sup>st</sup> June to the 21<sup>st</sup> September reduced the surface temperature by 30% and up to 62% for the 21<sup>st</sup> December. The prediction for the 21<sup>st</sup> March was about 40% lower than the surface temperature value obtained in the summertime. It was found that the RPSC performance based on Delta T can be observed highest during the summertime, demonstrating higher ambient temperature during the simulation time provides higher Delta T values. This simulation however was considered during noon time with less windy condition.

Figure 19: Delta T of RPSC performance based on seasonal changes

The comparative study of the surface temperature contour based on seasonal effect is presented in Figure 20. It was observed for all seasons that the surface temperature in the middle of the long canyon was the highest. The major factors that influence the surface temperature were the position of the sun and the irradiance which affects the ambient temperature. It was expected that the simulation of 21<sup>st</sup> December will predict the lowest temperature for the canyon surface which suggests that the system will not be effective during this month and other months with similar conditions. Overall, it showed that the simulation of the summer day with less wind condition was the most ample time to generate highest Delta T for potential energy.

Figure 20: Urban simulation by factoring season: (a) Spring (b) Summer (c) Autumn (d) Winter

## 5 Discussion and conclusion

Numerical study focusing on the 21<sup>st</sup> day of the summer June was carried out based on peak solar intensity by referencing to the maximum ambient temperature of the month. Investigation on the integrated road pavement solar collection (RPSC) system with an urban canyon model was discussed and was concluded in four sub-sections as below:

### **5.1 Method validation of integrated system based on de-coupled approach**

This study considered a simplified urban setting for the investigation of integrated urban RPSC system with the initial reason is to achieve high accuracy with reduced computational time. The characterisation of the model and the simulation setting were based on the published work of [39]. Validation of urban modelling with previous CFD model and wind tunnel experiment was carried out with most of the results are in good agreement. It could be mentioned that this validation took some efforts to match some results due to less meshing information found in the previous study. Hybrid meshing with inflation of First Layer Thickness setting was used to achieve low computational uncertainty and high speed computational simulation. The validation result of ground road surface demonstrated the difference between the simulated temperatures achieved highest which was 8.85% at the shadowed canyon road surface but less than 3% difference for the canyon hot side point and the external point. We highlighted the adjustment of the sunshine factor in ANSYS Fluent which had to be carried out before an optimal comparable result was determined in order to avoid extremely overestimated/underestimated temperatures at these specific ground road surface points. The adjusted sunshine factor of 0.25 provided optimal result for the validation of the ground surface absorbing heat from the solar radiation.

### **5.2 Effect of urban geometry on surface temperature**

The analysis showed that the effect of geometry on RPSC system performance was found to be significant, demonstrating building geometry causes unequal solar concentration distributed on the canyon ground surface as compared to no building geometry. At 13:00 hour, hotter surface temperature contours were found noticeable at the centre of the canyon towards Building A. The surface region next to Building B showed lower temperature contours, due to less solar concentration and the effect of building shadow. Average surface temperature at the nine selected points above 0.15m from the pipe location was determined to compare the two macro domains. The geometrical aspect of the urban canyon plays an important role for the unique performance of the surface. Critical aspect of the urban canyon in this study could be mentioned significant when the building length was north-south oriented, creating the nearest building wall to the wind inlet plane (Building A) as a wind blocking wall. The simulated wind flow had to cross over Building A and less wind velocity could be found inside the canyon with the limited canyon width setting. During the peak solar intensity when more heat can be absorbed, the necessity to reduce the surface temperature should be considered to eliminate the possible occurrence of surface and air based UHI effect. This type of geometry demonstrated the reduction in the rate of air-solid heat convection.

It was also confirmed lower temperature was spread from the northern and southern sides to the centre, showing the penetration of the lower temperature wind from the both ends in reducing the surface temperature through the circulated wind flow. Due to long canyon setting, the temperature for the road surface at the centre of the canyon was found higher as compared to the surface closer the openings. For an empty domain, direct solar radiation and convective heat transfer simplify the heat absorption to the surface. This can easily be predicted when similar temperature was found throughout the surface due to no building effect. It can be considered the comparative study of surface temperature in the two different domains setting was significant to evaluate the RPSC performance. Nevertheless, only one building orientation with one wind direction was used for this study.

### **5.3 RPSC system performance in two different domains**

Analysis of the RPSC system was performed for an approximate 10% at the centre area of canyon road surface. The initial reason of selecting the centre area for RPSC pipes embedment was to reduce the computational meshing for micro modelling while obtaining very fine mesh sizing. In our future study, simulation of full pipe length according to the canyon length should be considered. This is due to the noticeable lower temperature surfaces at the southern and northern region of the canyon road surface. Investigation of system performance was observed by calculating the potential temperature collection (PTC) and the surface temperature reduction (STR) based on Delta T. The simulation of the RPSC system on 21<sup>st</sup> June at 13:00 hour demonstrated that the RPSC system in the urban domain was 36.08% on average more effective in terms of thermal collection and 27.11% on average more surface reduction as compared to the rural/flat domain. Lower temperature was obtained for the shadowed surface which subsequently reduced the thermal performance of RPSC between 16.82% and 34.27%; demonstrating strong influence of the building geometry on the system performance.

### **5.4 Effect of daily solar intensity, wind velocity and seasonal changes on RPSC**

The investigations to predict the RPSC thermal behaviour in an urban configuration were carried out in three sub-sections. First, the effect of daily solar intensity was tested for the similar day as mentioned earlier. The steady state simulation took from 10:00 until 15:00 hours provided the results based on 3 selected pipes that represent very hot surface temperature, warm surface temperature and centre surface temperature. The graph of simulation demonstrated a bell curve plot; highlighting higher Delta T was obtained at noon and almost equally less in the morning and in the late afternoon. The temperature difference between the rural/flat pipe and the urban pipe B-5 that was located underneath the shadowed surface was obtained as high as 0.62K or 7.14%. More significant value was obtained for the pipes received higher temperature, C-1 and A-5 with 4.19K (48.95%) and 5.39K (63.26%) greater in the thermal performance, respectively. Overall, the simulations demonstrated the potential application and advantage of the system in daytime during the peak solar intensity.

Data from [46] showed that the unpredicted wind velocity can vary between 0 m/s to 10.3 m/s in the similar month. Therefore, the study demonstrated the impact of four different wind velocities: (i) 1 m/s, (ii) 2 m/s, (iii) 5 m/s and (iv) 10 m/s on the surface temperature, outlet water temperature and the Delta T. It was observed that the surface and the outlet water temperatures were significantly reduced as the wind velocity increases. The performance of the system was reduced up to 55.78% from the very low wind speed to the very high wind speed condition; limiting the application during the days with strong winds flow. Simulation of wind effect on the system performance can assist to provide necessary calibration of applying the system according to the climatic concern. Incorporating a control system which monitors the outdoor conditions (wind, solar, etc.) and optimises the system parameters could potentially improve the system efficiency.

The seasonal effect on the RPSC system performance was included for this study but is limited to compare the 21<sup>st</sup> of the month in four different seasons: (i) Spring – March, (ii) Summer – June, (iii) Autumn – September (iv) Winter – December. Based on the simulations, it was predicted that the summertime provided highest surface temperature as compared to the other three seasons, about 62%, 40% and 30% higher than winter, spring and autumn; respectively. The major factors which affect the reduction of the surface temperature were the position of the sun and the irradiance affecting the ambient temperature, although the simulation also found higher temperature contour at the centre of the canyon ground surface due to the wind effect across the building. Overall, summertime still provides the highest solar intensity that increases the system efficiency as compared to other seasons in the temperate climatic location.

## **6.0 Current limitation and future work**

Applying the RPSC system in an urban road with building infrastructures can be more challenging and complex, but significant value of the temperature collection at the urban outlet plane has potential for an extensive study. Integrating the building geometry as a variable for RPSC system investigation can be carried out by characterising the forms in respect to the complexity of an urban area. This study as we mentioned in the earlier section was limited to investigate the RPSC performance in two different scenarios by comparing the PTC and STR values. We also prolonged the analysis and discussion of the system performance in the unpredicted situation of high-low wind condition, daily time-dependent and seasonal changes but limited to certain day and month of temperate climatic location. For a sustainable use of the system, future investigation will require to consider the optimisation of the system when certain aspects were manipulated to enhance both energy collection and UHI ground surface temperature reduction. This study also enhances the importance to investigate the effect of the system in building thermal loads, which is required for our future studies. The aid of potential economic analysis of the conceptual system is another considerable study which can contribute in realising the system installation in an urban area.

## Acknowledgement

This research was supported by Energy 2050 team, The University of Sheffield. Special gratitude is also given to Malaysia government agency, Majlis Amanah Rakyat (MARA) for the 4 years scholarship of Malaysian postgraduate PhD study.

## References

- [1] Oke, T. R., Urban Climates and Global Environmental Change, Applied Climatology R.D. Thompson and A. Perry, Eds., Routledge (1999) pp. 273-287.
- [2] Sham, S., The Structure of the Kuala Lumpur Urban Heat Island and its Application in Air Quality Management and Planning, Urbanization and Eco- Development: With Special Reference to Kuala Lumpur, Institute of Advance Studies, Ed., University of Malaya Press, 1984a.
- [3] Rosenfeld, A.H., Akbari, H., Bretz, S., Fishman, B.L., Kurn, D. M., Sailor, D. and H. Taha, Mitigation of Urban Heat Island, Materials, Utility Programs, Updates, Energy and Buildings, 22 (1995) pp. 255–265.
- [4] Wilby, R. L., Past and Projected Trends in London’s Urban Heat Island. Weather, 58 (2003b) pp. 251–260.
- [5] Brain, S.J., Sensing Analysis of Residential Land Use, Forest Canopy Distribution and Surface Heat Island Formation in Atlanta Metropolitan Region, Ph. D. thesis, Georgia Institute of Technology, Georgia, Atlanta, 2001.
- [6] Elsayed, I.S., C.M. Che, The Effects of Traffic Activity on the Intensity of the Urban Heat Island: A Case Study on the City of Kuala Lumpur, Malaysia, In the Proceedings of the Second International Green Energy Conference, Ontario, Canada., 2006.
- [7] Akhbari, H., Energy Saving Potentials and Air Quality Benefits of Urban Heat Island Mitigation (2005), <http://www.osti.gov/bridge/servlets/purl/860475-U1H-WIq/860475.PDF>
- [8] NOAA. Natural Disaster Survey Report: July 1995 Heat Wave (1995), <http://www.nws.noaa.gov/om/assessments/pdfs/heat95.pdf>
- [9] Green Power, Report on Urban Heat Island Effect in Hong Kong (2012), [http://www.greenpower.org.hk/html/download/concern/gp\\_urban\\_heat\\_island\\_report\\_2012.pdf](http://www.greenpower.org.hk/html/download/concern/gp_urban_heat_island_report_2012.pdf)
- [10] Berdahl, P., S., Bretz, Preliminary Survey of the Solar Reflectance of Cool Roofing Materials, Energy and Buildings 25 (1997) pp. 149-158.
- [11] Erell, E., P. David Boneh, D., Kutiel, P., Bar, Effect of High-Albedo Materials on Pedestrian Heat Stress in Urban Street Canyons, Urban Climate (2013).
- [12] Taha, H., Urban Climates and Heat Islands: Albedo, Evapotranspiration, and Anthropogenic Heat, Energy and Buildings 25 (1997), pp 99-103.
- [13] Rosenfield, A.H., J.J. Romm, H. Akhbari, M. Pomerantz. Cool Communities: Strategies for Heat Islands Mitigation and Smog Reduction, Energy and Building. 28 (1998) pp.51-62.
- [14] Tan S., T. Fwa, Influence of Pavement Materials on the Thermal Environment of Outdoor Spaces. Building and Environment, Vol. 27, No. 3 (1992) pp. 289-295.
- [15] E. Bilgen, M.-A. Richard, Horizontal Concrete Slabs As Passive Solar Collector, Solar Energy Vol. 72, No. 5 (2001) pp. 405–413, 2002.
- [16] Loomans, M., H. Oversloot, A.D. Bondt, R. Jansen, H.V., Rij, Design Tool for the Thermal Energy Potential of Asphalt Pavements, Eighth International IBPSA Conference Eindhoven, Netherlands, August 11-14, 2003.
- [17] Luca J., and D. Mrawira, New Measurement of Thermal Properties of Superpave Asphalt Concrete, Journal of Materials in Civil Engineering 17 (2005) pp. 72-79.
- [18] Qin, Y., J.E., Hiller, Modelling Temperature Distribution in Rigid Pavement Slabs: Impact of Air Temperature, Construction and Building Materials 25 (2011) pp. 3753-3761.

- [19] Karunaratne, A., W., Mamparachchi, Modelling of Thermal Effects due to Solar Radiation on Concrete Pavements, University of Moratuwa, Sri Lanka, 2010.
- [20] Hall, M.R., P.K., Dehdezi, A.R., Dawson, J., Grenfell, R., Isola, Influence of the Thermophysical Properties of Pavement Materials on the Evolution of Temperature Depth Profiles in Different Climatic Regions, *Journal of Materials in Civil Engineering*, 24 (2012) pp. 32-47.
- [21] Bobes-Jesus, V., P., Pascual-Muñoz, D., Castro-Fresno, J., Rodriguez-Hernandez, Asphalt Solar Collectors: A Literature Review, *Applied Energy* 102 (2013) pp. 962–970.
- [22] Hasebe, M., Y., Kamikawa, S., Meiarashi, Thermoelectric Generators into Solar Thermal Energy in Heated Road Pavement, International Conference on Thermoelectrics, 2006.
- [23] Yue, W.S., Z., QiYang, D., YingNa, S., PeiDong, Unidirectional Heat-Transfer Asphalt Pavement for Mitigating the Urban Heat Island Effect, *Journal of Materials in Civil Engineering* 26 (2014) pp. 812-821.
- [24] Gao, Q., Y., Huang, M., Li, Y., Liu, Y.Y. Yan, Experimental Study of Slab Solar Collection on the Hydronic System of Road, *Solar Energy* 84 (2010) pp. 2096-2102.
- [25] Wang, H., S., Wu, M., Chen, Y., Zhang, Numerical Simulation on the Thermal Response of the Heat-Conducting Asphalt Pavement, *The Royal Swedish Academy of Sciences Phys. Scr.* T139 (2010) 014041.
- [26] Bijsterveld W.T., L.J.M., Houben, A., Scarpas, A.A.A., Molenaar, Using Pavement as Solar Collector. Effect on Pavement Temperature and Structural Response, *Transport Research Record* 1778 (17) (2001) pp. 140–148.
- [27] Chen, M., S., Wu, H., Wang, J., Zhang, Study of Ice and Snow Melting Process on Conductive Asphalt Solar Collector, *Solar Energy Materials & Solar Cells* 95 (2011) pp. 3241–3250.
- [28] Wu, S., M. Chen, J., Zhang, Laboratory Investigation into Thermal Response of Asphalt Pavements as Solar Collector by Application of Small-Scale Slabs, *Applied Thermal Engineering* 31 (2011) pp. 1582-1587.
- [29] Wu, S., M., Chen, H., Wang, and Y., Zhang, Laboratory Study on Solar Collector of Thermal Conductive Asphalt Concrete, *International Journal of Pavement Research and Technology*. 2(4) (2009) pp. 130-136.
- [30] Maggiotto, G., R. Buccolieri, M.A., Santo, Validation of Temperature-Perturbation and CFD-based Modelling for the Prediction of the Thermal Urban Environment, The Lecce (IT) Case Study. *Environmental Modelling & Software* 60 (2014) pp. 69-83.
- [31] Pascual-Muñoz, P., D. Castro-Fresno, P. Serrano-Bravo, A. Alonso-Estébanez, Thermal and Hydraulic Analysis of Multilayered Asphalt Pavements as Active Solar Collectors, *Applied Energy* 111 (2013) pp. 324–332.
- [32] García, A., M.N., Partl, How to Transform an Asphalt Concrete Pavement into a Solar Turbine, *Applied Energy* 119 (2014) pp. 431–437.
- [33] Sailor, D.J., H. Fan. Modelling the Diurnal Variability of Effective Albedo for Cities, *Atmospheric Environment*. 36 (2002) pp. 713-725.
- [34] Levermore, G.J., H.K.W., Cheung, S Low Order Canyon Model to Estimate the Influence of Canyon Shape on the Maximum Urban Heat Island Effect, *Building Serv. Eng. Res. Technol.* 33, 4 (2012) pp. 371-385.
- [35] Georgakis, CH., S., Zoras, M., Santamouris, Studying the Effect of “Cool” Coatings in Street Urban Canyons and its Potential As A Heat Island Mitigation Technique, *Sustainable Cities and Society*, 13 (2014), pp. 20-31.
- [36] Allegrini, J., V., Dorer, J., Carmeliet, Coupled CFD, Radiation and Building Energy Model for Studying Heat Flux in An Urban Environment with Generic Building Configurations, *Sustainable Cities and Society*, In Press, Corrected Proof (2015).
- [37] Takahashi, K., H., Yoshida, Y., Tanaka, N., Aotake, F., Wang, Measurement of Thermal Environment in Kyoto City and its Prediction by CFD Simulation, *Energy and Building* 36 (2004) pp. 771-779.
- [38] Rajagopalan, P., K.C., Lim, E., Jamei, Urban Heat Island and Wind Flow Characteristics of a Tropical City, *Solar Energy* 107 (2014) pp. 159-170.
- [39] S. Bottillo, A.D.L., Vollaro, G. Galli, A. Vallati, Fluid Dynamic and Heat Transfer Parameters in an Urban Canyon, *Solar Energy* 99 (2014) pp. 1-10.

- [40] Allegrini, J., V., Dorer, T., Defraeye, J., Carmeliet, An Adaptive Temperature Wall Function for Mixed Convective Flows at Exterior Surfaces of Buildings in Street Canyons, *Building and Environment* 49 (2012) pp. 55-66.
- [41] Ansys Fluent version 14.0.0, 2011. User's Guide
- [42] Uehara, K., S., Murakami, S., Oikawa, S., Wakamatsu, Wind Tunnel Experiments on How Thermal Stratification Affects in and Above Urban Street Canyons, *Atmospheric Environment* 34 (2000) pp. 1553-1562.
- [43] Memon, R.A., D. Y.C. Leung, C. Liu, Effects of Building Aspect Ratio and Wind Speed on Air Temperatures in Urban-Like Street Canyons, *Building and Environment* 45 (2010) pp. 175-188
- [44] Bulletin of the Polytechnic Institute, Technical University Georghie Asachi, Recommendation for Pipes Selections in Heating and Cooling Systems (2009). Available: <http://www.ce.tuiasi.ro/~bipcons/Archive/62.pdf>
- [45] Allegrini, J., V. Dorer, J. Carmeliet, Influence of the Urban Microclimate in Street Canyons on the Energy Demand for Space Cooling and Heating of Buildings, *Energy and Buildings* 55 (2012) pp. 823-832.
- [46] Wunderground.com "Forecast for Cavaria Con Premezzo, Varese – Summary June 21, 2015 until July 21, 2015", 2015. Available: <http://www.wunderground.com/personal-weather-station/dashboard?ID=IVARESEC3#history/s20150622/e20150721/mmonth> [Accessed: 17-August-2015]
- [47] Wunderground.com "Forecast for Cavaria Con Premezzo, Varese – Summary February 19, 2015 until March 21, 2015", 2015. Available: <http://www.wunderground.com/personal-weather-station/dashboard?ID=IVARESEC3#history/s20150219/e20150321/mmonth> [Accessed: 17-August-2015]
- [48] Wunderground.com "Forecast for Cavaria Con Premezzo, Varese – Summary December 21, 2014 until January 20, 2014", 2014. Available: <http://www.wunderground.com/personal-weather-station/dashboard?ID=IVARESEC3#history/s20141221/e20150120/mmonth> [Accessed: 17-August-2015]
- [49] Wunderground.com "Forecast for Cavaria Con Premezzo, Varese – Summary September 21, 2014 until October 21, 2014", 2014. Available: <http://www.wunderground.com/personal-weather-station/dashboard?ID=IVARESEC3#history/s20140921/e20141021/mmonth> [Accessed: 17-August-2015]
- [50] Anniballe, R., S., Bonafoni, M., Pichierri, Spatial and Temporal Trends of the Surface and Air Heat Island over Milan using MODIS Data, *Remote Sensing of Environment*, 150 (2014) pp. 163-171.
- [51] O'Connor, D., J., K., Calautit, B., R., Hughes, A Study of Passive Ventilation Integrated with Heat Recovery, *Energy and Buildings* 82 (2014) pp. 799-811.

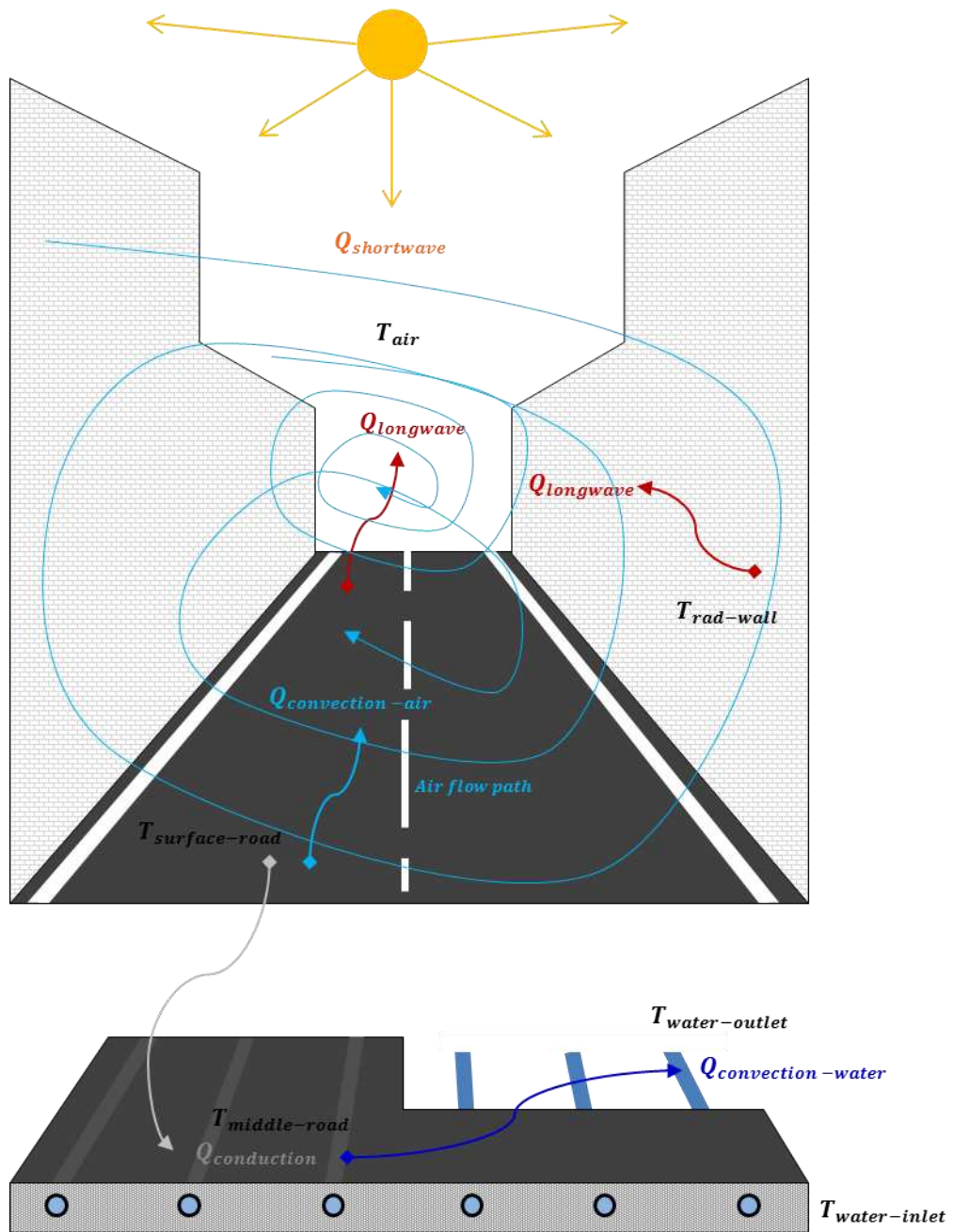


Figure 1: Schematic diagram of RPSC system in urban environment

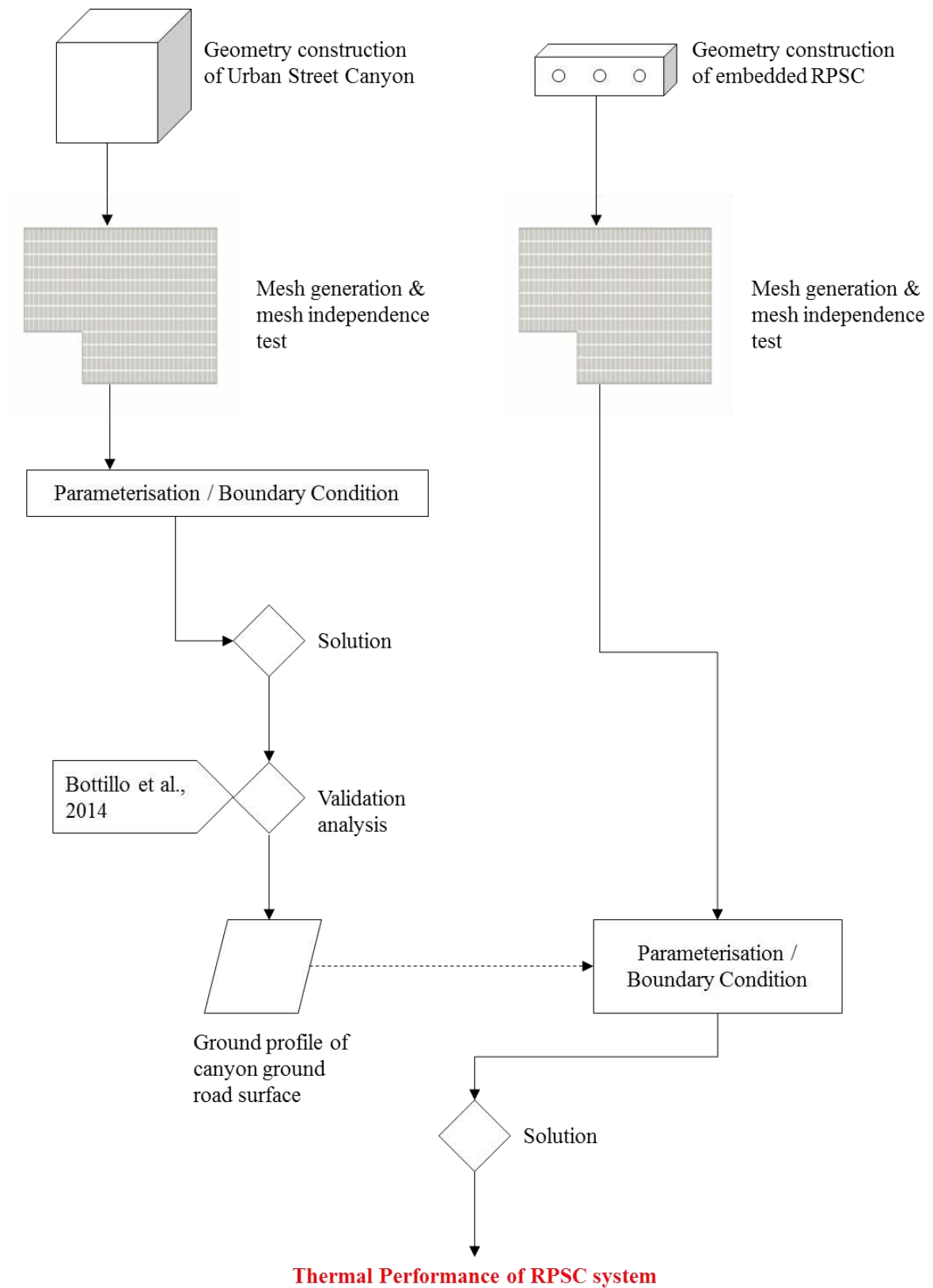


Figure 2: Methodology chart of the de-coupled approach CFD model

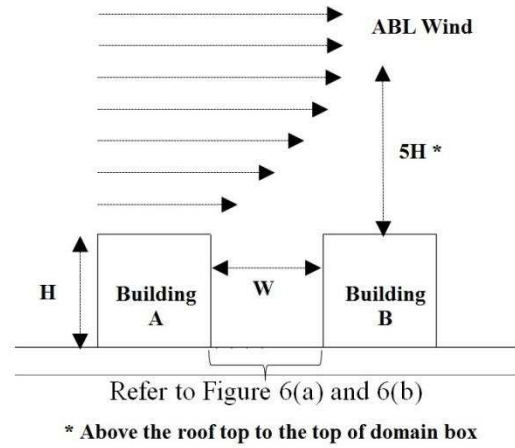


Figure 3: Schematic diagram of RPSC-canyon system

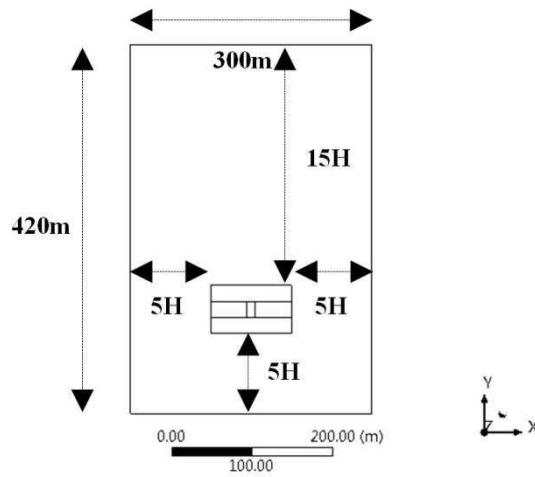
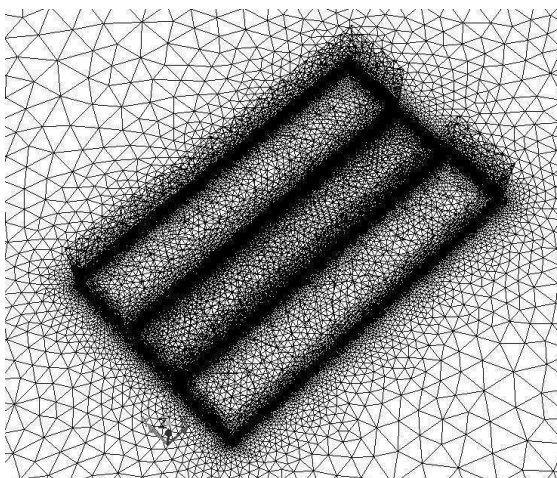
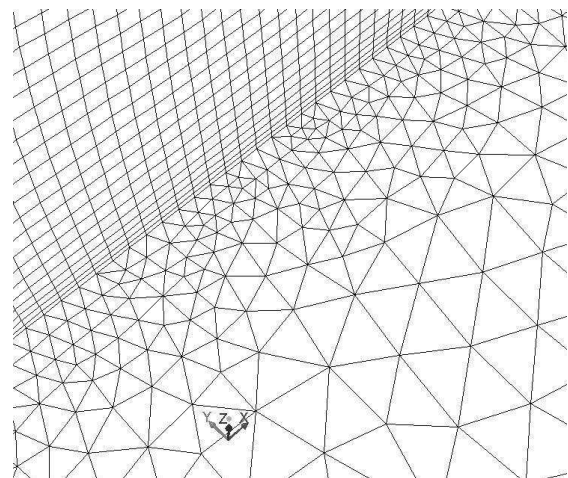


Figure 4: Urban domain description based on height from plan view



(a)



(b)

Figure 5: Perspective view of (a) canyon mesh generation (b) hexahedral mesh at building wall

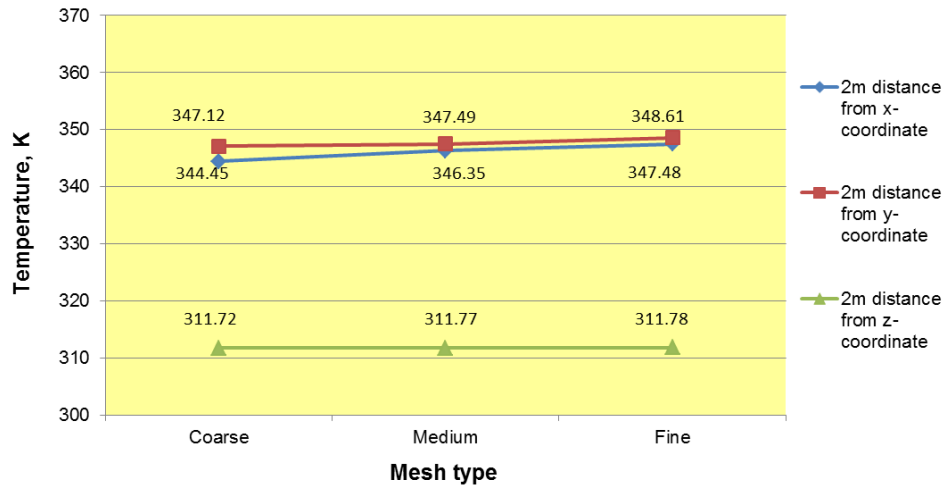


Figure 6: Mesh independent test

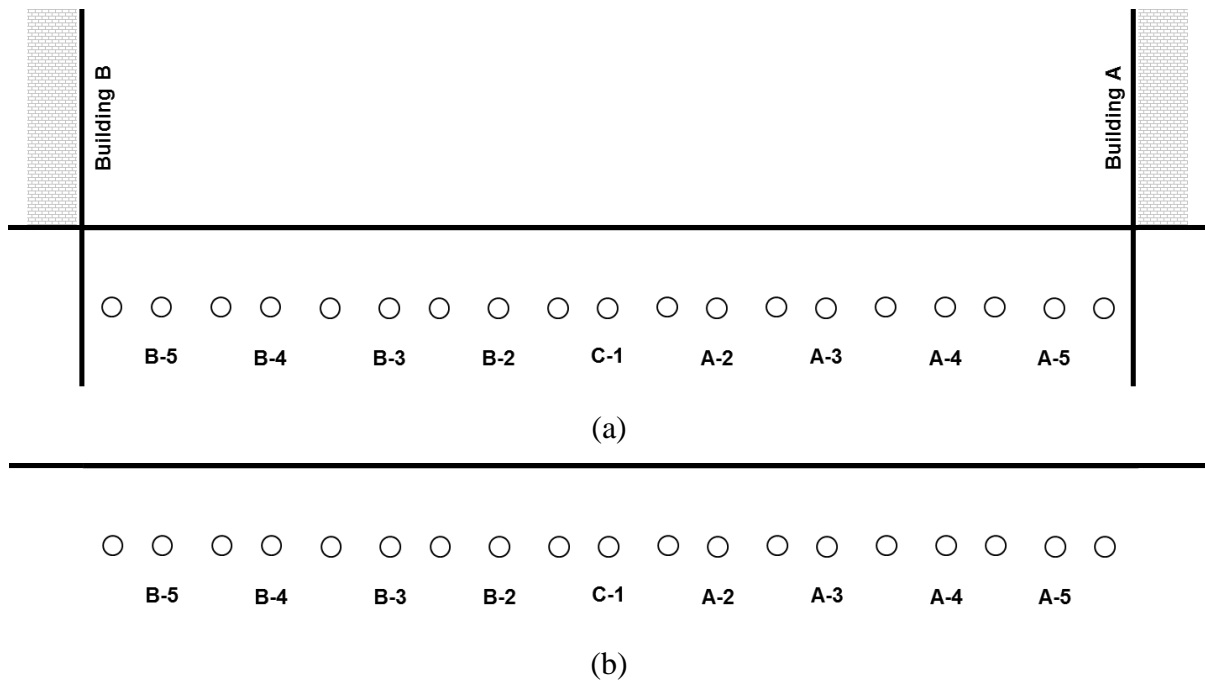


Figure 7: RPSC pipes embedded inside (a) a canyon road surface (b) flat surface without canyon

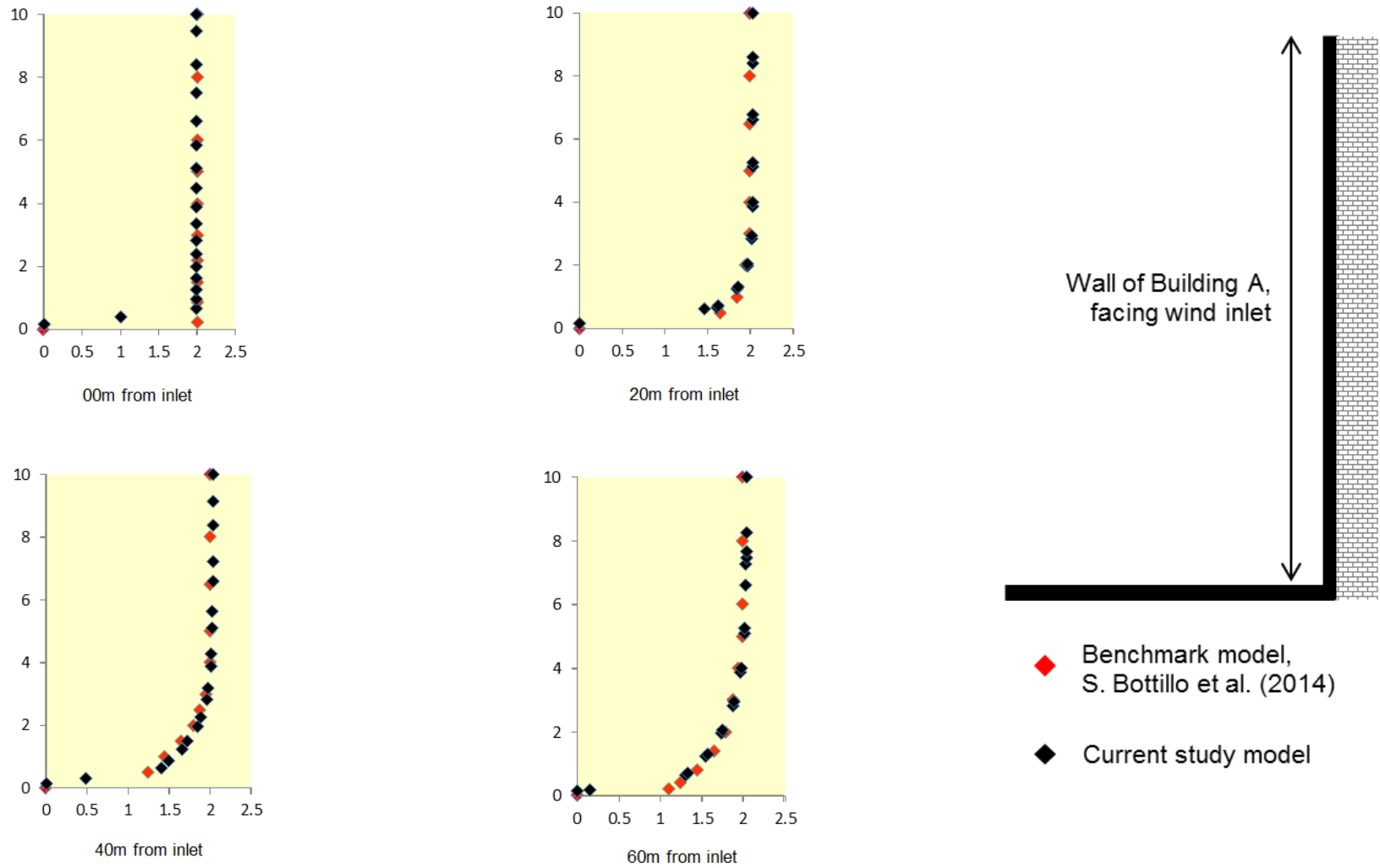


Figure 8: Validation of wind velocity at four locations based on y-direction

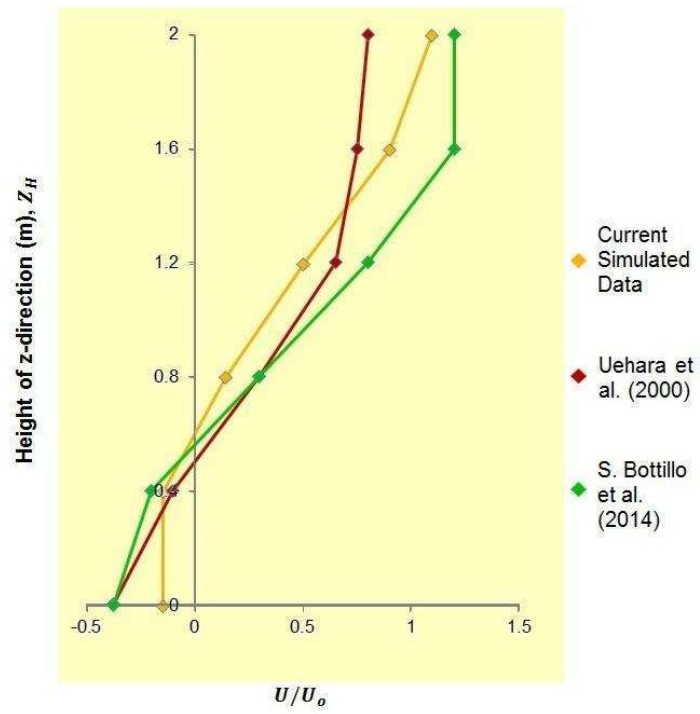


Figure 9: Canyon wind velocity profile

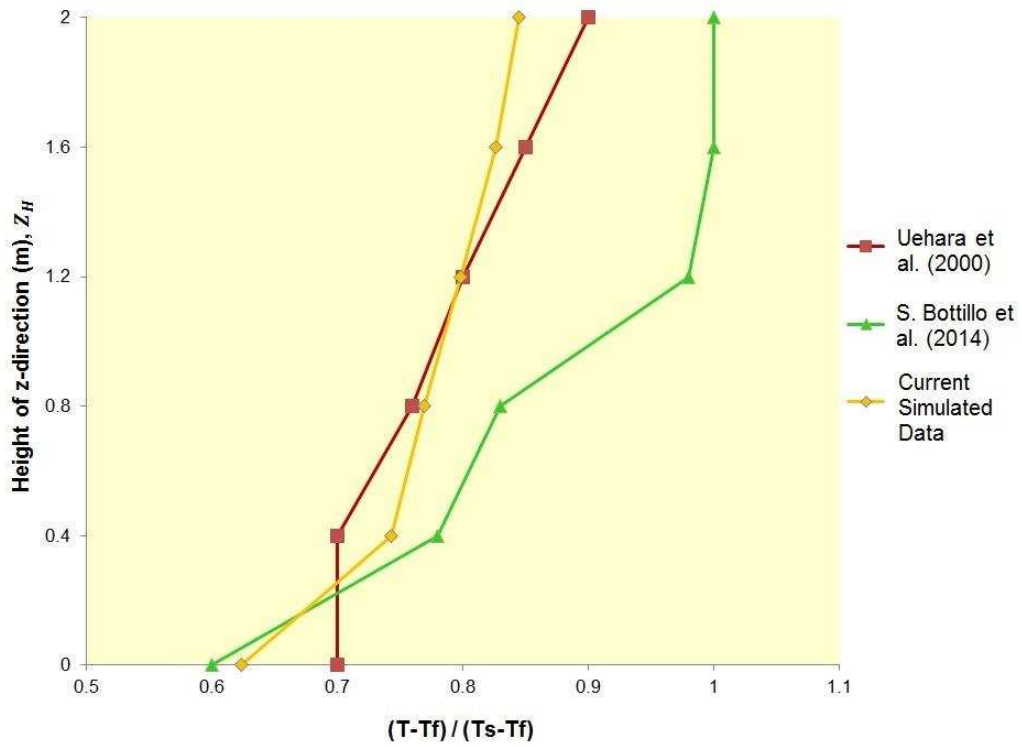


Figure 10: Canyon air temperature profile

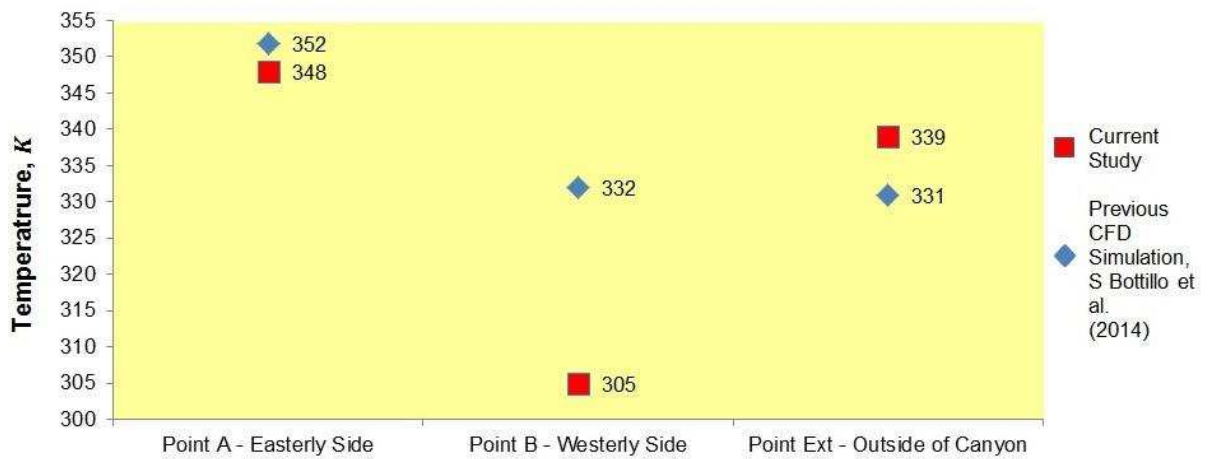


Figure 11: Validation of the ground road surface temperatures

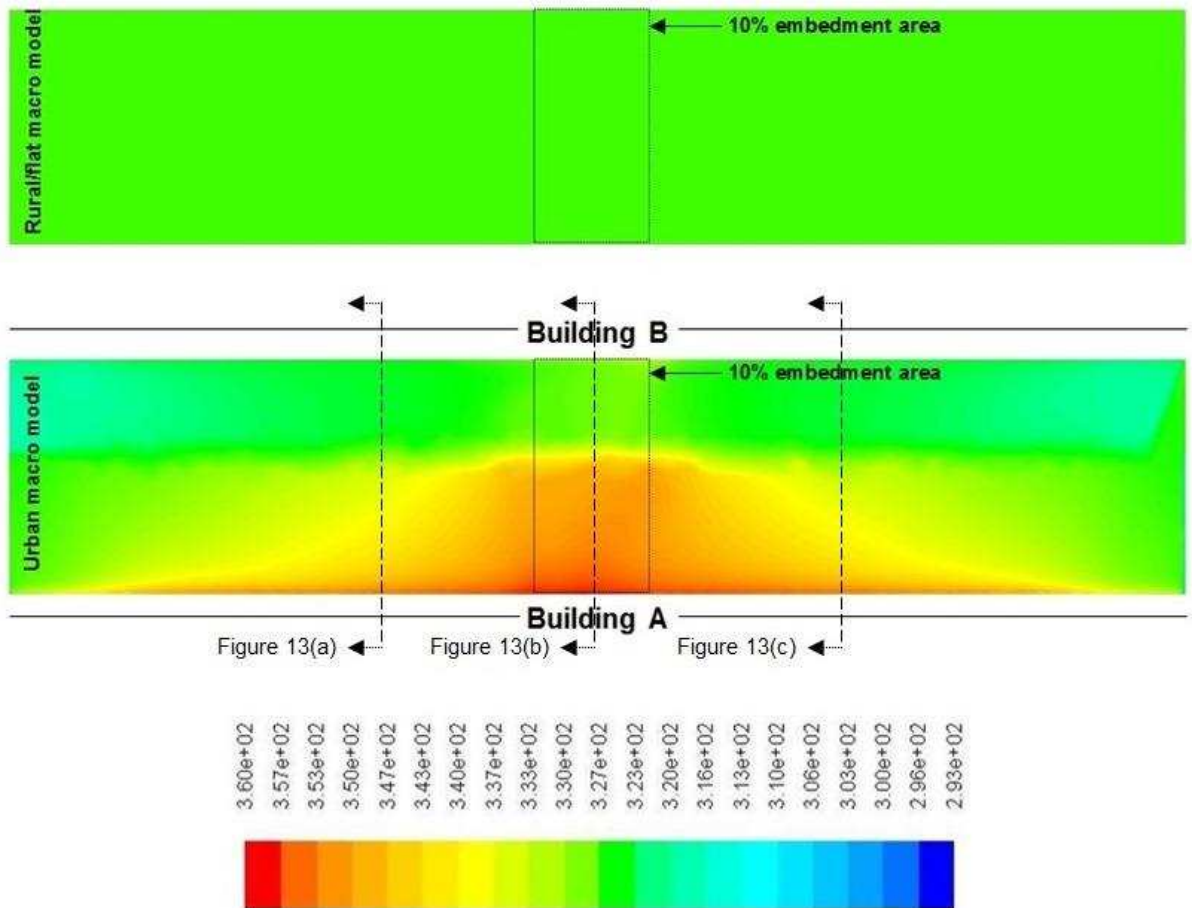


Figure 12: Simulated ground surface temperature in urban and rural/flat macro domains

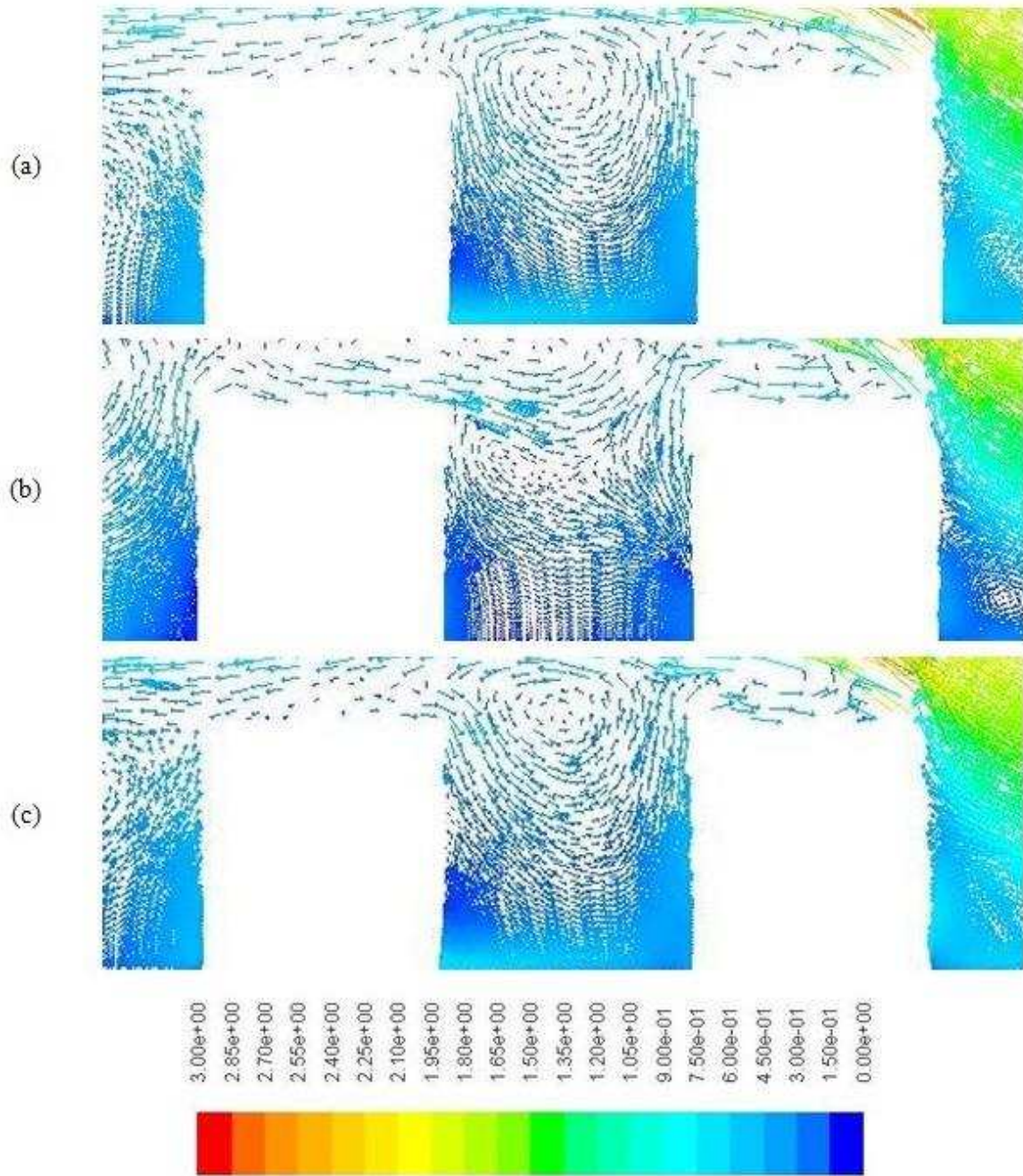


Figure 13: Air profile at (a) 120m x-direction, (b) 150m x-direction (c) 180m x-direction

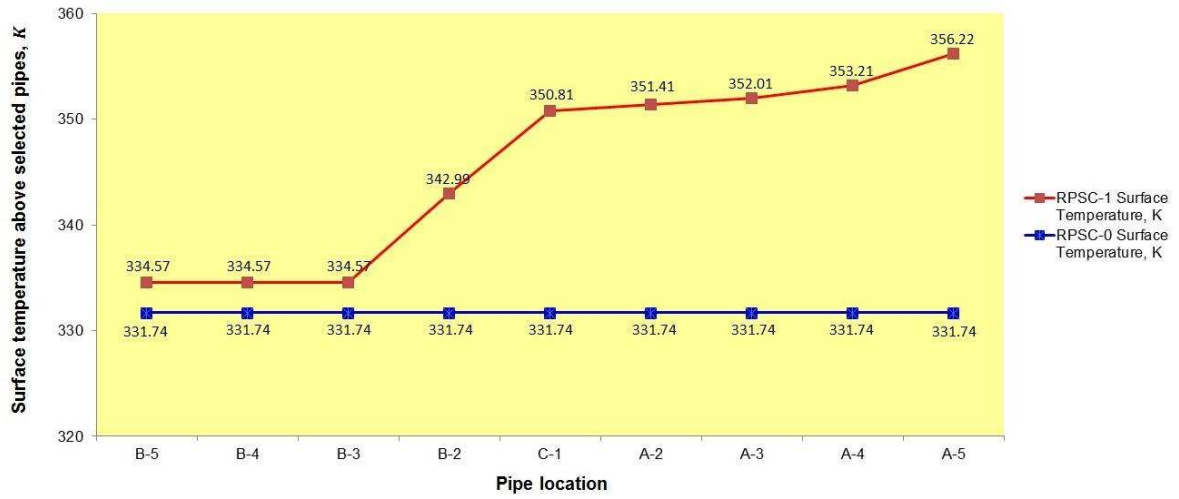


Figure 14: Ground surface temperature 0.15m above selected pipe location at 13:00 hour

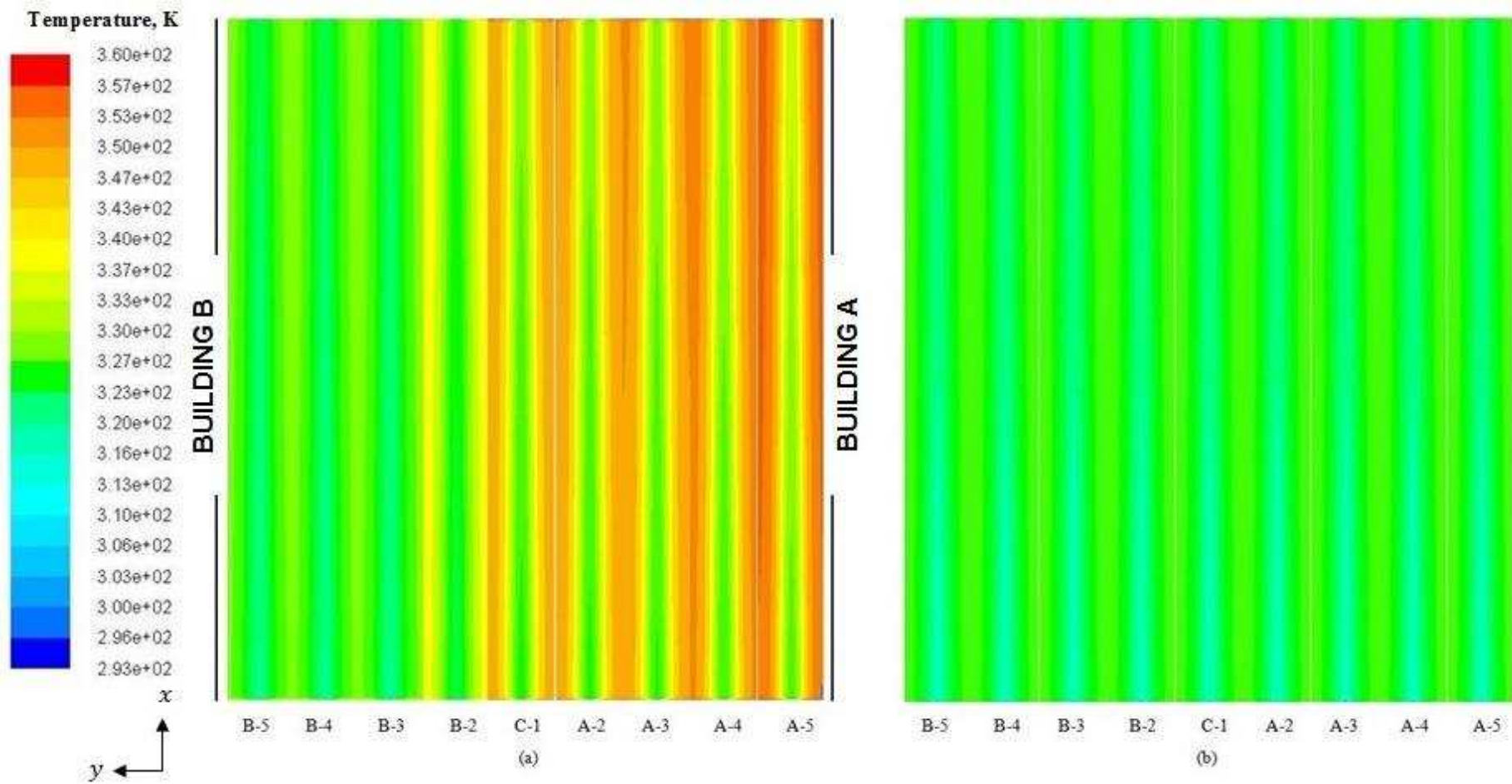
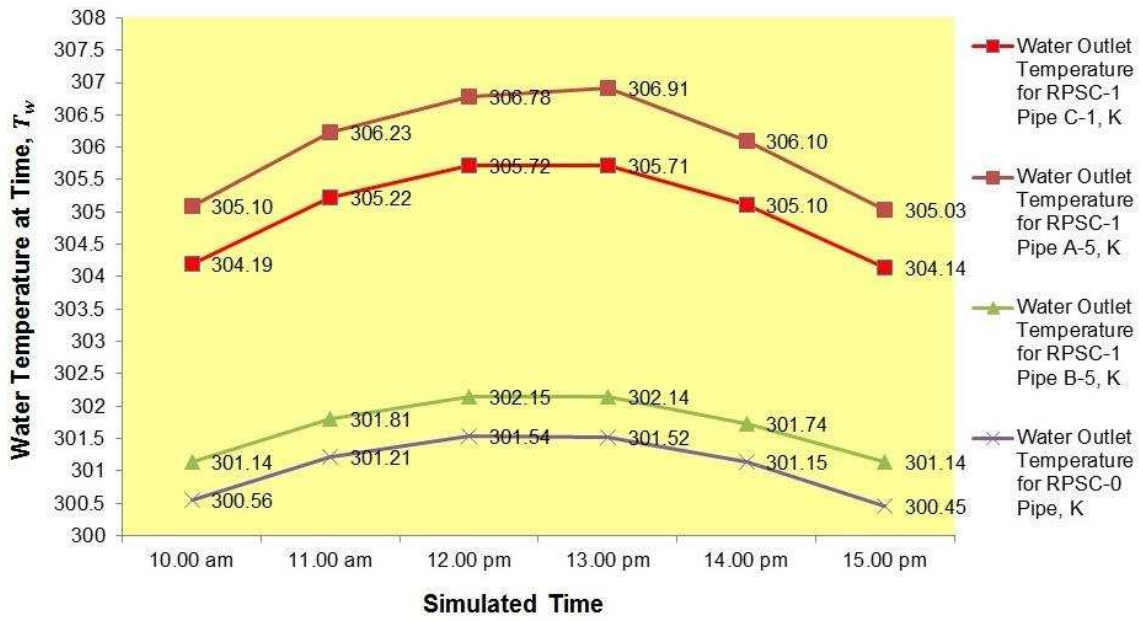
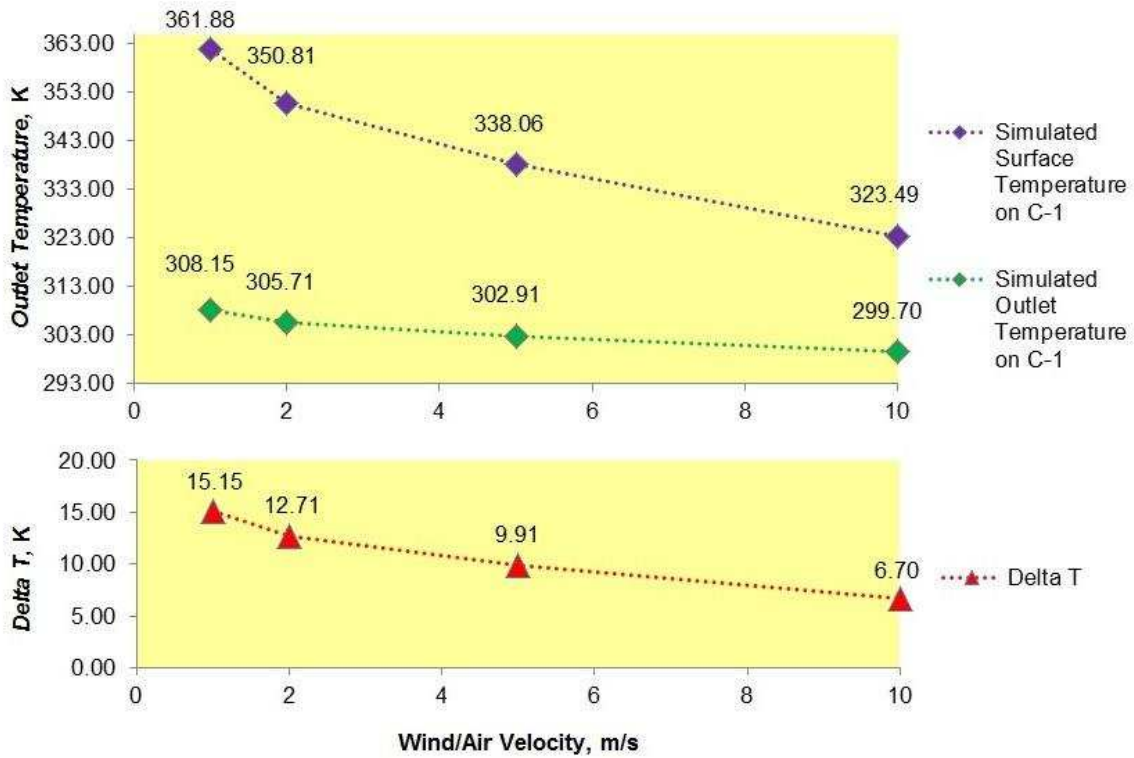


Figure 15: Surface temperature after RPSC simulation at 0.15m below pipes for: (a) urban macro domain (b) rural/flat macro domain



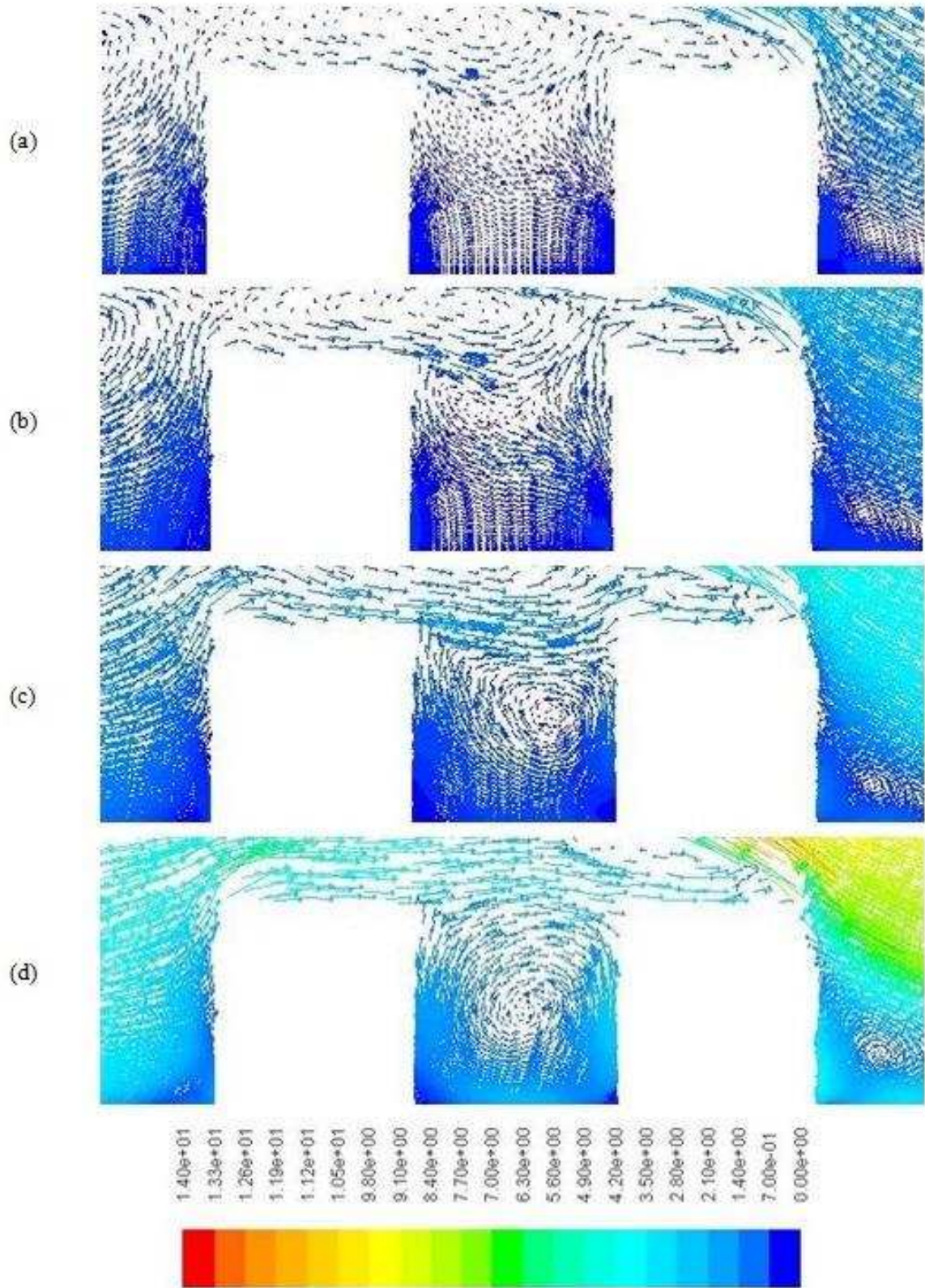
1  
2  
3

Figure 16: Solar intensity study on outlet water temperature

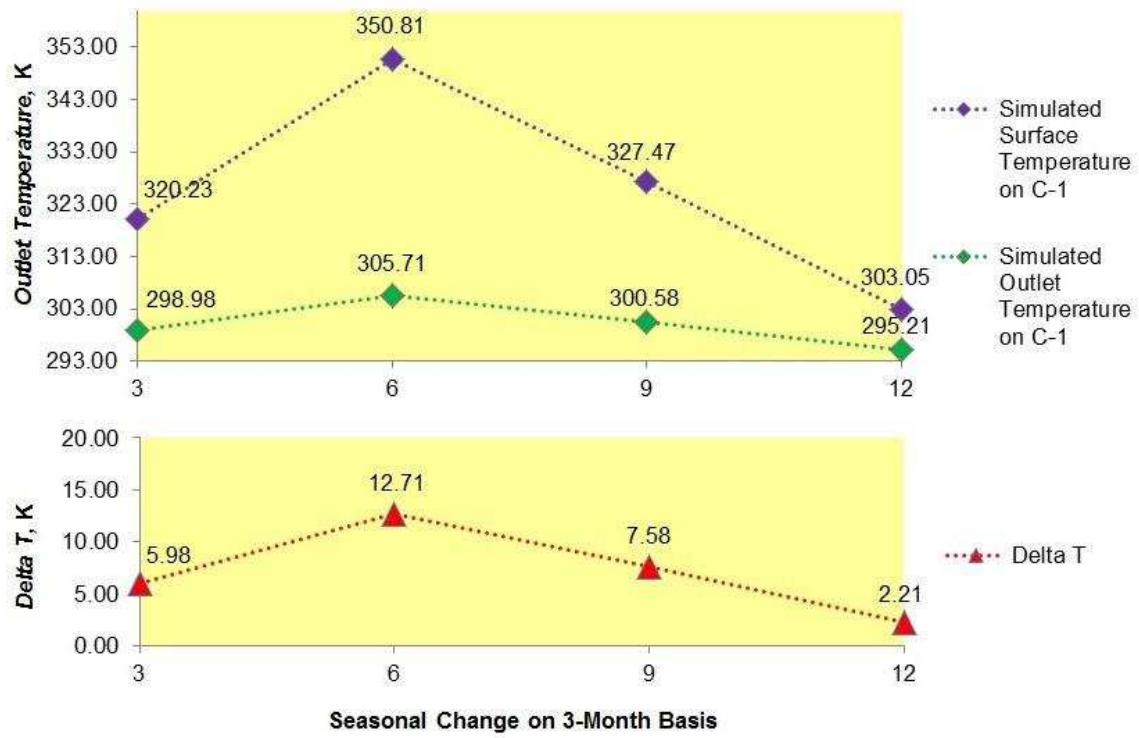


4  
5

Figure 17: Delta T of RPSC performance based on wind factor



1 Figure 18: Cross-sectional plane of velocity vector inside the canyon:  
 2 (a) 1 m/s (b) 2 m/s (c) 5 m/s (d) 10 m/s



1

2

Figure 19: Delta T of RPSC performance based on seasonal changes

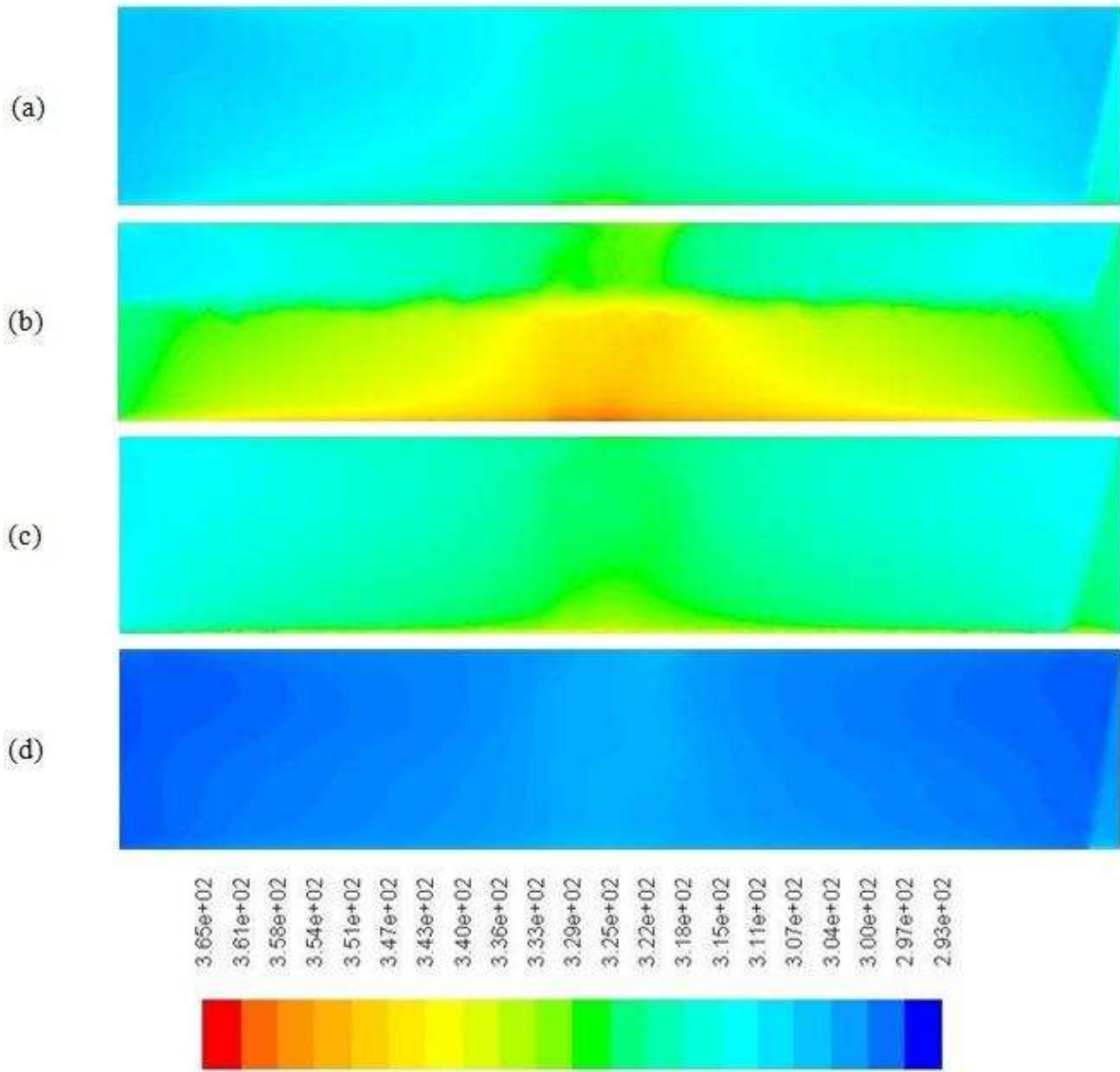


Figure 20: Urban simulation by factoring season: (a) Spring (b) Summer (c) Autumn (d) Winter

1  
2  
3  
4